NAST

Nonadiabatic Statistical Theory

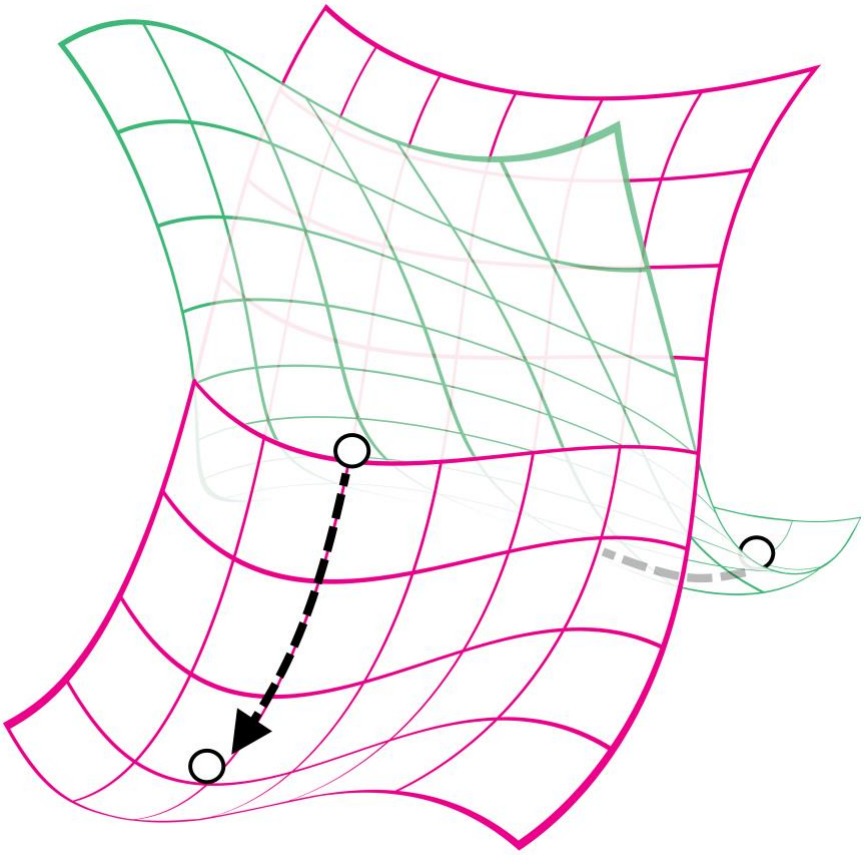

User manual and installation guide

University of Nevada, Reno

Version 2021.1

MIT License

If you use the NAST package, please site the following publications:

1) Lykhin, A. O.; Kaliakin, D. S.; DePolo, G. E.; Kuzubov, A. A.; Varganov, S. A. Nonadiabatic Transition State Theory: Application to Intersystem Crossings in the Active Sites of Metal-Sulfur Proteins. *Int. J. Quantum Chem.* **2016**, *116* (10), 750–761. https://doi.org/10.1002/qua.25124.

2) Lykhin, A. O.; Varganov, S. A. Intersystem Crossing in Tunneling Regime: $T_1 \rightarrow S_0$ Relaxation in Thiophosgene. *Phys. Chem. Chem. Phys.* **2020**, *22* (10), 5500–5508. https://doi.org/10.1039/c9cp06956a.

Table of content

1. Installation guide

• Quick start

The NAST package can be installed with the following Linux commands:

```
$ ./configure.py --lib_path=path_to_math_library
$ make
$ make clean
$ cd checkcomp
$ ./checknast
```

Here, **path_to_math_library** is the path to preinstalled math library. The **make** command creates the executable **nast.x**. The **checknast** script tests the installation by running several examples of NAST calculations.

• Installation overview

The NAST package is distributed as a source code written in modern Fortran for Linux distributions.

○ Prerequisites

The following prerequisites are strongly recommended:

1. Fortran compiler. The NAST source code has been successfully compiled using GNU Fortran (GCC) 4.8.5, GNU Fortran (GCC) 8.2.0 and ifort (IFORT) 13.0.0.
2. Math library. NAST has been successfully tested with the Intel® Math Kernel Library (MKL) versions 2018.2.199 – 2018.4.274, 2019.0.177 – 2019.5.281 and 2020.0.166.
3. Python interpreter, version 2.4 or greater (usually included in any modern Linux distribution).

○ Configuration

NAST is configured using the Python script **configure.py**. The default configuration settings can be overwritten using the following flags:

--fc=... **Fortran compiler**

--fcflags="..." List of compiler flags
--lib_path=... Path to math library
--libs="..." Library files to be linked

A typical script execution will look like the following:

$ ./configure.py --fc=... --fcflags="..." --lib_path=... --libs="..."

The default values for --fc, --fcflags, --lib_path and --libs can be printed by executing **./configure.py --help**. If multiple compilers are available, the full path should be provided (e.g. **--fc=/path/to/bin/gfortran**). **Executing ./configure.py with all defaults is equivalent to**

$ ./configure.py --fc=gfortran --fcflags="-O0 -g -fcheck=bounds -fcheck=all -C" --lib_path=/usr/local/include/mkl/lib/intel64 --libs="-lmkl_intel_lp64 -lmkl_sequential -lmkl_core -lpthread -lm -ldl"

- ### Configuration notes

1. The default --fcflags are set for the GNU Fortran compiler **gfortran**. For the Intel Fortran compiler **ifort**, the user must set the corresponding Intel flags. If defaults are used, the best-case scenario is that these flags will be ignored with a warning (e.g. **ifort: command line warning #10006: ignoring unknown option '-fcheck=bounds'**).
2. The default for the MKL flag is **lmkl_intel_lp64**, even if **gfortran** is used as a compiler. Perhaps the proper combination would be **gfortran** and **-lmkl_gf_lp64**. However, in practice, both combinations produce the same result.
3. Recommendations for the GNU and Intel compilers:

   GNU Fortran: **--fcflags="-g -fcheck=bounds -fcheck=all -Wall"**
   Intel Fortran: **--fcflags= "-g -ftz -auto"**

- ### Compilation

The **configure.py** script creates **Makefile**. The Linux command **make** uses the configuration information stored in the **Makefile** to compile the NAST source files and create the executable **nast.x**.

$ make
$ make clean (optional – deletes temporary files)

- ### Compilation notes

1. If necessary, **Makefile** can be edited manually.
2. For the executable **nast.x** to run, the environmental variables PATH and LD_LIBRARY_PATH must contain path to the math library. For example, if bash shell is used, these variables can be set in **.bash_profile** as:

   export PATH = $PATH:/…/compilers_and_libraries_20XX.X.XXX/linux/bin

   export LD_LIBRARY_PATH = $LD_LIBRARY_PATH:/ …/linux/mkl/lib/intel64

3. If multiple versions of MKL are installed, to avoid possible conflicts, the environmental variable **LIB** should be specified. For example, it can be set in **.bash_profile** as:

   export LIB=/specific_version /linux/mkl/include/
   specific_version/linux/mkl/bin/mklvars.sh intel64

- **Testing**

To test a new NAST build, several test examples are available in the **/path/to/nast/checkcomp** directory. Executing the **checknast** script will invoke a loop over the test examples.

$ ./checknast
Sat Aug 28 12:33:18 PDT 2021

An empty directory is being created for:

---- exam01_1 ----
---- exam01_2 ----
---- exam02_1 ----
---- exam02_2 ----
---- exam03 ----
---- exam04 ----
---- exam05 ----
---- exam06 ----
---- exam07 ----

Done creating directories. Running the tests now.

---- Testing exam01._1inp ----
…… Passed

---- Testing exam01_2.inp ----
…… Passed

```
        and so on
Done with tests
```

All tests should terminate with **Passed**. Failed tests may indicate problems with new NAST build.

2. Nonadiabatic Statistical Theory

2.1. Introduction

The nonadiabatic statistical theory (NAST) describes kinetics of nonradiative transitions between a pair of electronic states with different spin multiplicities.[1,2] A central NAST approximation is that the interstate transitions effectively take place at the minimum energy crossing point (MECP) on the crossing seam of coupled potential energy surfaces (PESs) of two spin states.[3,4] The main capabilities of NAST, implemented in this package, include calculations of microcanonical and canonical rate constants, as well as microcanonical and velocity-averaged transition probabilities. The NAST package has two modes of operation. First is the forward rate constant calculations. In this mode, a standard NAST run requires knowledge of molecular properties only at reactant and MECP. A more sophisticated optional run will require knowledge about points along the potentials, which represent the minimum energy paths that connect MECP with reactant and product. Use of such potentials ensures higher accuracy of rate constant calculations. The second operation mode is calculation of the forward and reverse rate constants in the same run. Such run will require molecular properties at reactant, MECP and product. Note that in this mode of operation, reactant and product are defined as minima of higher-energy and lower-energy states, correspondingly. Therefore, the forward transitions correspond to relaxation process. Note that in this mode, sophisticated calculations employing explicit crossing potentials are currently available for forward transitions only.

In the limit of an adiabatic reaction proceeding on a single electronic state, NAST reduces to the traditional transition state theory (TST).[1] The corresponding TST rate constants can be calculated using the NAST package.

2.3. Main equations

Microcanonical rate constant. The central quantity of NAST is the microcanonical rate constant of the transitions between two electronic states of different spin multiplicities:

$$k(E) = \sigma \frac{N_{\mathrm{X}}(E)}{h\rho_{\mathrm{R}}(E)}, \tag{2.1}$$

$$N_{\mathrm{X}}(E) = \int_0^E \rho_{\mathrm{X}}(E-\varepsilon_\perp)P(\varepsilon_\perp)d\varepsilon_\perp, \tag{2.2}$$

$$\sigma = \frac{\sigma_R}{\sigma_X}\gamma_X, \tag{2.3}$$

where $N_{\mathrm{X}}(E)$ is the effective number of states at the MECP, ρ_{R} and ρ_{X} are the densities of rovibrational states at reactant and MECP, respectively, and h is Planck's constant. The interstate transition probability $P(\varepsilon_{\perp})$ is a function of the energy $\varepsilon_{\perp}$ partitioned in the reaction coordinate orthogonal to the crossing seam. The reaction path degeneracy σ is defined in terms of the symmetry numbers of reactant (σ_R) and MECP (σ_{X}), and the number of chiral MECP isomers (γ_{X}).[5]

The densities of vibrational and rotational states are obtained in the rigid rotor and harmonic oscillator approximations. To calculate vibrational density of states, we implement the direct counting algorithm:[6]

```
    define E_max as the energy limit
do loop over all vibrational frequencies of reactant (MECP):
  do j = 1 to number 3N-6 (3N-5 for linear molecule or 3N-7 at MECP)
    set counter k = 0
    do while frequency(j)*k < E_max
      k = k +1;  e_bin = ceil (frequency(j)*k)
      vib_density(e_bin) = vib_density(e_bin) + 1
    end do
      To account for ZPE:
    vib_density(1) = vib_density(1) + 1
  end do
```

To calculate rotational density of states, we use classical assymetric top model:

$$\rho_{\mathrm{rot}}(E_{\mathrm{rot}}) = \frac{4\sqrt{2E_{\mathrm{rot}}}}{\hbar^3}\sqrt{I_{\mathrm{A}}I_{\mathrm{B}}I_{\mathrm{C}}}, \tag{2.4}$$

where I_{A}, I_{B} and I_{C} are the principal moments of inertia of a molecule.

To calculate rovibrational density of states, we use the convolution formula:

$$\rho(E) = \int_0^E \rho_{\mathrm{vib}}\,(E - E_{\mathrm{rot}})\rho_{\mathrm{rot}}(E_{\mathrm{rot}})dE_{\mathrm{rot}}, \tag{2.5}$$

where ρ_{vib} and ρ_{rot} are the vibrational and rotational densities of states defined above, correspondingly.

Microcanonical ISC probabilities. Prediction of the transition probability in equation 2.2 is central to calculation of the rate constants. Typical models, used to derive probability expressions, assume 1-D linear potentials in the vicinity of crossing. Derived from these models are the Landau-Zener (LZ) and Weak Coupling (WC) transition probabilities[2], implemented in this package:

$$P_{\mathrm{LZ}}(\varepsilon_{\perp}) = p_{\mathrm{LZ}} + (1 - p_{\mathrm{LZ}})p_{\mathrm{LZ}} = 2p_{\mathrm{LZ}} - {p_{\mathrm{LZ}}}^2, \tag{2.6}$$

$$p_{\mathrm{LZ}}(\varepsilon_{\perp}) = 1 - \exp\left(-\frac{2\pi H_{SO}^2}{\hbar|\Delta\mathbf{g}|}\sqrt{\frac{\mu_{\perp}}{2(\varepsilon_{\perp} - E_X)}}\right), \tag{2.7}$$

$$P_{\mathrm{WC}}(\varepsilon_{\perp}) = 4\pi^2 H_{\mathrm{SO}}^2 \left(\frac{2\mu_{\perp}}{\hbar^2\bar{\mathbf{g}}|\Delta\mathbf{g}|}\right)^{\frac{2}{3}} \mathrm{Ai}^2\left(-(\varepsilon_{\perp} - E_X)\left(\frac{2\mu_{\perp}|\Delta\mathbf{g}|^2}{\hbar^2\bar{\mathbf{g}}^4}\right)^{\frac{1}{3}}\right), \tag{2.8}$$

where p_{LZ} is the single-passage LZ probability, H_{SO} is the spin-orbit coupling constant, $\hbar$ is reduced Planck's constant. The norm of the gradient parallel to the reaction coordinate $|\Delta\mathbf{g}| = |\mathbf{g}_1 - \mathbf{g}_2|$ and the mean gradient $\bar{\mathbf{g}} = (|\mathbf{g}_1||\mathbf{g}_2|)^{1/2}$ are defined in terms of the gradients of two crossing PESs at MECP, $\mathbf{g}_1$ and $\mathbf{g}_2$. In equations 2.7 and 2.8, $\mu_{\perp}$ is the reduced mass for the motion along the reaction coordinate and E_{X} is the MECP energy barrier with respect to the reactant minimum. In equation 2.8 Ai is the Airy function. The WC formula readily accounts for quantum tunneling and for double passage through the seam. The double-passage form of the LZ probability is given in equation 2.6. More information on derivation and applicability limits of Landau-Zener and Weak Coupling formulae can be elsewhere[7–12]. The LZ probability is defined only at the reaction energy ε_⊥ above MECP, and therefore does not account for quantum tunneling through the MECP barrier. In addition, the LZ probability formula does not describe the quantum interference between primary and secondary passages at MECP.[1] On the other hand, these two quantum effects are included in the WC probability formula that has been extensively used.[11,13,14] However, both the LZ and WC formulas are only valid within the limited region of the parameters $\varepsilon_{\perp}$, $\mu_{\perp}$, H_{SO} and the energy gradients.

To account for ZPE, the MECP energy can be redefined as $E_{\mathrm{X}} \rightarrow E_{\mathrm{X}} + ZPE_{\mathrm{X}} - ZPE_{\mathrm{R}}$. The ZPE_{R} and ZPE_{X} are the zero-point energies at the reactant minimum and MECP, respectively, and for nonlinear molecules are

$$ZPE_{\mathrm{R}} = \frac{1}{2}\sum_{\mathrm{i}=1}^{3\mathrm{N}-6} \hbar\omega_{\mathrm{i}}^{\mathrm{R}}, \tag{2.9}$$

$$ZPE_{\mathrm{X}} = \frac{1}{2}\sum_{\mathrm{i}=1}^{3\mathrm{N}-7} \hbar\omega_{\mathrm{i}}^{\mathrm{X}}, \tag{2.10}$$

where ω_i are the frequencies of the fundamental transitions. For non-linear molecules, *i* in equation 2.9 runs over $3N-6$ vibrational DOF, while only $3N-7$ transverse DOF contribute to the ZPE at MECP. Note that the use of ZPE_{X} at the classical turning point along the minimum energy path is equivalent to the zero-curvature tunneling approximation in TST, where the density of the rovibrational states is approximated by the density at TS and the effective TS barrier is reduced by the difference between ZPE_{R} and ZPE_{TS}.

Zhu-Nakamura transition probabilities. A more sophisticated approach to predict transition probabilities was suggested by Zhu and Nakamura.[2,15,16] In their approach, predicting the transition probability at each energy $\varepsilon_\perp$ requires knowledge of abscisse points along the reaction coordinate for each of two crossing potentials. Therefore, the use of the Zhu-Nakamura (ZN) transition probability requires two analytical crossing potentials. These potentials can be obtained in either spin-diabatic or spin-adiabatic representation. In addition, Zhu-Nakamura explicitly distinguishes two possible intersection types: sloped intersection ($\mathbf{g}_1 \cdot \mathbf{g}_2 > 0$) and peaked intersection ($\mathbf{g}_1 \cdot \mathbf{g}_2 < 0$):

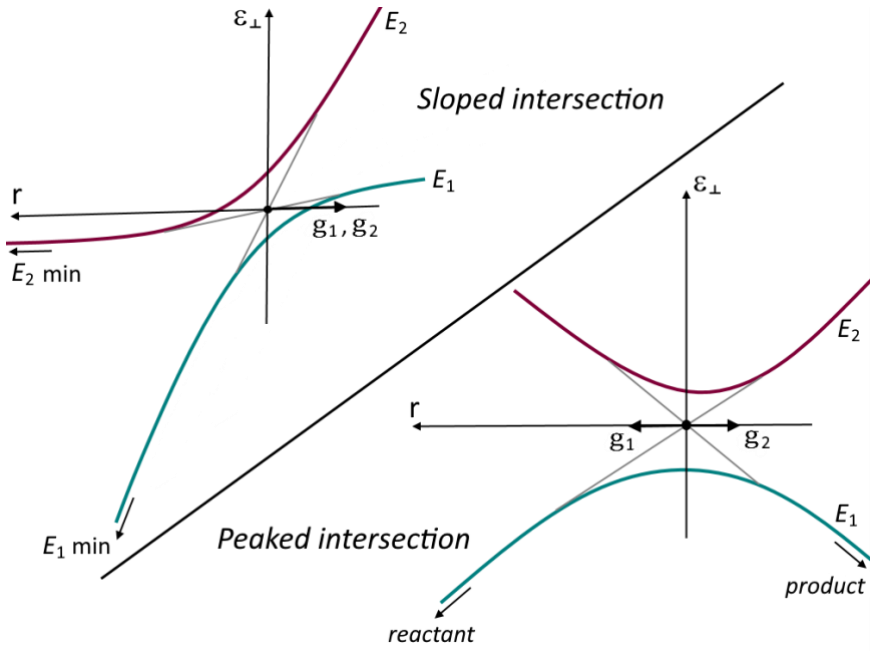

Figure 1. Sloped (upper left) and peaked (lower right) intersections of potentials of two states along the one-dimensional reaction coordinate r. The E_1 and E_2 electronic states are shown in spin-diabatic (grey) and spin-adiabatic (coloured curves) representations.

Note: In the current implementation, ZN transition probability is available for sloped-type transitions only in the spin-adiabatic representation. However, most of the electronic structure packages, which can used to collect the NAST input data, work in spin-diabatic representation. Therefore, spin-adiabatic implementation of ZN requires adiabatization of the crossing potentials. For adiabatization, we use the constant value of the spin-orbit coupling, as calculated at the MECP, along the potentials:

$$\widehat{H}_0 + \widehat{H}_{\mathrm{SOC}} = \begin{pmatrix} E_1(r) & H_{\mathrm{SOC}} \\ H_{\mathrm{SOC}} & E_2(r) \end{pmatrix}, \tag{2.11}$$

where E_1 and E_2 are the spin-diabatic energies of two electronic states with arbitrary spin multiplicities, r is arc length along the minimum-energy path in mass-scaled coordinates[17] with the reduced mass μ set to 1 amu, and H_{SO} is spin-orbit coupling constant computed at MECP. Note: SOC is not the only coupling mechanism between states of different spin multiplicity. However, it is usually the largest in magnitude and thus is considered in the first place. Therefore, the SOC selection rules apply when modeling coupling between states. Due to these selection rules, and neglecting higher order terms, the non-zero coupling remains only between singlet-triplet, triplet-quintet, doublet-quartet, quartet-sextet, etc. pairs.

The probability of transition at any energy $\varepsilon_\perp = E$, $P_{\mathrm{ZN}}(\varepsilon_\perp)$, is parametrized with a set of a, b and d spin-adiabatic parameters and σ, δ and ψ phases (Figure 2):

$$P_{\mathrm{ZN}}(\varepsilon_\perp) = 4p_{\mathrm{ZN}}(1 - p_{\mathrm{ZN}})\sin^2(\psi), \tag{2.12 A}$$

$$p_{\mathrm{ZN}} = p_{\mathrm{ZN}}(a, b, d, \sigma, \delta, \psi), \tag{2.12 B}$$

$$a^2 = (d^2 - 1)^{1/2} \frac{\hbar^2}{\mu(t_2^0 - t_1^0)^2(E_2(r_0) - E_1(r_0))}, \tag{2.12 C}$$

$$b^2(\varepsilon_\perp) = (d^2 - 1)^{1/2} \frac{\varepsilon_\perp - (E_2(r_0) + E_1(r_0))/2}{(E_2(r_0) - E_1(r_0))/2}, \tag{2.12 D}$$

$$d^2 = \frac{(E_2(t_1^0) - E_1(t_1^0))((E_2(t_2^0) - E_1(t_2^0))}{(E_2(r_0) - E_1(r_0))^2}, \tag{2.12 E}$$

$$\sigma \approx \delta \approx Integral(r, r_0, t_1, t_2), \tag{2.12 F}$$

$$\psi = f(\sigma, \delta), \tag{2.12 G}$$

where P_{ZN} is the Zhu-Nakamura double passage probability, p_{ZN} is a single passage probability and ψ is the overall transition phase. p_{ZN} probability is parametrized as a function of a, b, d, σ, δ and ψ. All the parameters are functions of the r_0, t_1^0, t_2^0, t_1 and t_2 turning points along two spin-adiabatic potentials. The r_0, t_1^0, t_2^0 turning points are calculated at the

MECP, whereas t_1 and t_2 are energy specific and are sought for at every energy $\varepsilon_\perp$ (Figure 2):

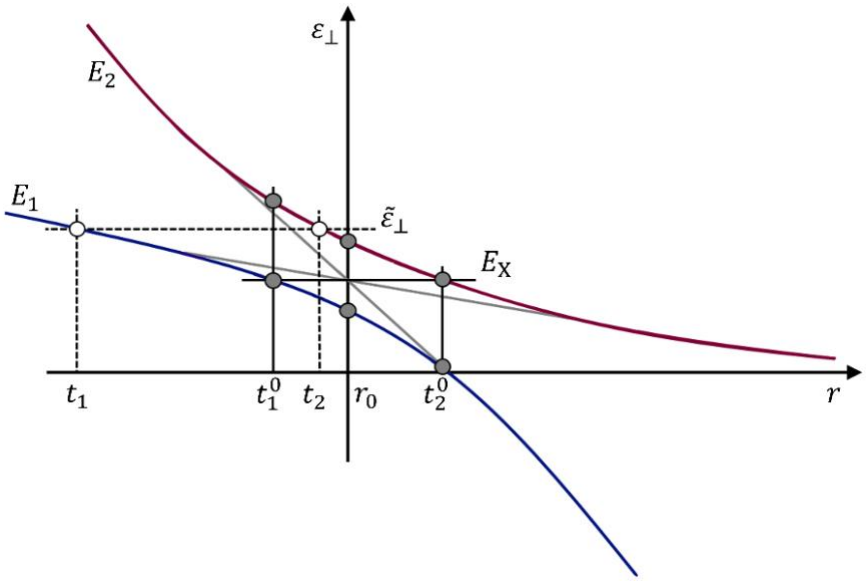

Figure 2. Sloped intersection of two spin-adiabatic potentials with the energies E_1 (blue) and E_2 (red). The classical turning points r_0, t_1^0, t_2^0, t_1 and t_2 are defined in the text.

More details about the Zhu-Nakamura theory can be found in our recent paper[12].

Canonical NAST. A canonical, temperature-dependent, rate constant can be obtained by averaging the microcanonical rate constant (Eq. 1) over the internal energy Boltzmann distribution, leading to the following expression:

$$k(T) = \frac{\sigma}{hQ_{\mathrm{R}}(T)} \int_0^\infty N_X(E) e^{-E/k_B T} dE, \tag{2.13}$$

$$Q_{\mathrm{R}}(T) = \int_0^\infty \rho_R(E)\, e^{-E/k_B T}\, dE, \tag{2.14}$$

where Q_{R} is the partition function of the reactant, T is the temperature, and k_B is the Boltzmann constant.

A special case would be calculation of canonical rate constants in solution phase, which is invoked with the **solution = .true.** keyword set in the input file. We approximate solution phase calculations by assuming no bulk rotation takes place and thus exclude calculation of the rotational density of states. Thus, we supersede the rovibrational density of states with

vibrational density in equations 2.1, 2.2 and 2.14. We also calculate the LZ and WC velocity-averaged transition probabilities obtained by averaging microcanonical probabilities over the Maxwell-Boltzmann and Kuki[18] distributions of velocity v:

$$\langle p_{\mathrm{LZ}}(T)\rangle_{\mathrm{MB}} = 1 - \left(\frac{2}{\pi k_B T}\right)^{\frac{1}{2}} \int_0^{\infty} \exp\left(-\frac{2\pi H_{\mathrm{SO}}^2 \mu_{\perp}^{\frac{1}{2}}}{\hbar|\Delta\mathbf{g}|v}\right) \exp\left(-\frac{v^2}{2k_B T}\right) dv, \tag{2.15}$$

$$\langle p_{\mathrm{LZ}}(T)\rangle_{\mathrm{K}} = 1 - \frac{1}{k_B T} \int_0^{\infty} v \exp\left(-\frac{2\pi H_{\mathrm{SO}}^2 \mu_{\perp}^{\frac{1}{2}}}{\hbar|\Delta\mathbf{g}|v}\right) \exp\left(-\frac{v^2}{2k_B T}\right) dv, \tag{2.16}$$

$$\langle P_{\mathrm{WC}}(T)\rangle_{\mathrm{MB}} = \alpha \left(\frac{2}{\pi k_B T}\right)^{\frac{1}{2}} \int_0^{\infty} \mathrm{Ai}^2\left(-\frac{1}{2}v^2 \mu_{\perp}\gamma\right) \exp\left(-\frac{v^2}{2k_B T}\right) dv, \tag{2.17}$$

$$\langle P_{\mathrm{WC}}(T)\rangle_{\mathrm{K}} = \frac{\alpha}{k_B T} \int_0^{\infty} v\, \mathrm{Ai}^2\left(-\frac{1}{2}v^2 \mu_{\perp}\gamma\right) \exp\left(-\frac{v^2}{2k_B T}\right) dv, \tag{2.18}$$

$$a = 4\pi^2 H_{\mathrm{SO}}^2 \left(\frac{2\mu_{\perp}}{\hbar^2 \bar{\mathbf{g}}|\Delta\mathbf{g}|}\right)^{\frac{2}{3}}, \tag{2.19}$$

$$\gamma = \left(\frac{2\mu_{\perp}|\Delta\mathbf{g}|^2}{\hbar^2 \bar{\mathbf{g}}^4}\right)^{\frac{1}{3}}. \tag{2.20}$$

It is important to note that, in contrast to the microcanonical probabilities, these velocity-averaged WC probabilities do not account for quantum tunneling.

Rate constants and transition probabilities between individual MS components. A simple approach to model transitions between electronic states with different spin quantum numbers S and S' is to calculate the effective probabilities and rates accounting for all M_S components of these spin multiplets. In this approach, the effective SOC, also called SOC constant, is obtained as the RMS of the couplings between individual M_S components,

$$H_{\mathrm{SO}} = \left(\sum_{M_S=-S}^{S} \sum_{M_S'=-S'}^{S'} \left|\langle S, M_S|\hat{H}_{\mathrm{SO}}|S', M_{S'}\rangle\right|^2\right)^{1/2}, \tag{2.21}$$

where $\widehat{H}_{\mathrm{SO}}$ is the spin-orbit operator, for example, from the Breit-Pauli Hamiltonian.[19] This approach is easy to justify for the case of singlet-triplet crossing where the energy gap between the two spin-adiabatic states at the MECP is equal to $2H_{\mathrm{SO}}$[1]. However, for the states with higher spin multiplicities, for example a triplet-quintet crossing, there are multiple energy gaps between the adiabatic states. Therefore, employing a single effective SOC to calculate the transition probability and rate constant is not well-justified.

This issue can be resolved by calculating the rate constants and transition probabilities between individual M_S components of the spin multiplets using the LZ formula (Eqs. 4 and 5). As an example, for a singlet-triplet crossing, the non-zero spin-orbit coupling matrix elements are

$$z = \langle 0,0|\widehat{H}_{\mathrm{SO}}|1,-1\rangle, \qquad ib = \langle 0,0|\widehat{H}_{\mathrm{SO}}|1,0\rangle, \qquad z^* = \langle 0,0|\widehat{H}_{\mathrm{SO}}|1,+1\rangle, \tag{2.22}$$

where z and z^* are complex conjugate to each other, and b is real. The single-passage LZ probabilities $p_{LZ}^{M_S,M_{S'}}(\varepsilon_\perp)$ between the components M_S and $M_{S'}$ of the spin states $S = 0$ and S'=1 read

$$p_{LZ}^{0,-1}(\varepsilon_\perp) = p_{LZ}^{0,+1}(\varepsilon_\perp) = 1 - \exp\left(-\frac{2\pi zz^*}{\hbar|\Delta\mathbf{g}|}\sqrt{\frac{\mu_\perp}{2(\varepsilon_\perp - E_{\mathrm{X}})}}\right), \tag{2.23}$$

$$p_{LZ}^{0,0}(\varepsilon_\perp) = 1 - \exp\left(-\frac{2\pi b^2}{\hbar|\Delta\mathbf{g}|}\sqrt{\frac{\mu_\perp}{2(\varepsilon_\perp - E_{\mathrm{X}})}}\right). \tag{2.24}$$

The double-passage probabilities $P_{LZ}^{0,\pm1}$ and $P_{LZ}^{0,0}$ can be obtained from the single passage probabilities using Eq. (5) and employed to calculate the microcanonical rate constants between individual M_S components,

$$k_{0,\pm1}(E) = \frac{\sigma}{h\,\rho_{\mathrm{R}}(E)}\int_0^E \rho_{\mathrm{X}}(E-\varepsilon_\perp)P_{LZ}^{0,\pm1}(\varepsilon_\perp)d\varepsilon_\perp, \tag{2.25}$$

$$k_{0,0}(E) = \frac{\sigma}{h\,\rho_{\mathrm{R}}(E)}\int_0^E \rho_{\mathrm{X}}(E-\varepsilon_\perp)P_{LZ}^{0,0}(\varepsilon_\perp)d\varepsilon_\perp. \tag{2.26}$$

The probabilities and rate constants between individual M_S components can be calculated for any pair of spin states with $|S - S'|$ =1.

Transition state theory rate constants. For adiabatic reactions, both microcanonical and canonical NAST rate constants can be reduced to the traditional TST rate constants by replacing MECP with transition state (TS) and the transition probability in equation 2.2 with the Heaviside step function.[20] The canonical TST rate constant $k(T)$, obtained by averaging the microcanonical constants over Boltzmann distribution of the reactants density of states, is equivalent to the traditional analytical TST formula:[1]

$$k(T) = \sigma \frac{k_B T}{h} \frac{Q_{\mathrm{TS}}}{Q_{\mathrm{R}}} e^{-E_{\mathrm{TS}}/k_{\mathrm{B}}T}, \qquad (2.27)$$

where Q_{TS} and Q_{R} are partition functions of TS and reactant, correspondingly.

2.2. NAST input data and electronic structure calculations

Prerequisite to NAST calculations is collection of the input data. Here, we list all the data required for NAST (TST) calculation. **Note: input data should be given in units specified below. Conversion to atomic units will be done automatically by program.**

NAST input data:

- $\boldsymbol{\nu}_{\mathrm{R}}$ – vibrational frequencies of the reactant, (cm^{-1})
- $\boldsymbol{I}_{\mathrm{R}}$ – principal moments of inertia of the reactant, (amu × $bohr^2$)
- $\boldsymbol{\nu}_{\mathrm{X}}$ – vibrational frequencies of the MECP, (cm^{-1})
- $\boldsymbol{I}_{\mathrm{X}}$ – principal moments of inertia of the MECP, (amu × $bohr^2$)
- $\mu_{\perp}$ – reduced mass (amu) along the vibrational mode associated with the reaction coordinate at the MECP. This vibrational mode is an analog of the vibrational mode for a transition state, which connects reactants and products in transition state theory.
- E_{X} – electronic energy of MECP, (hartree)
- E_{R} – electronic energy of reactant, (hartree)
- E_{P} – electronic energy of product, (hartree) (optional)
- $|\Delta\mathbf{g}| = |\mathbf{g}_1 - \mathbf{g}_2|$ – norm of the gradient parallel to the reaction coordinate at the MECP, (hartree/bohr)
- $\bar{\mathbf{g}} = (|\mathbf{g}_1||\mathbf{g}_2|)^{1/2}$ – mean gradient (hartree/bohr)
- SOC – the spin-orbit coupling (SOC) constant (cm^{-1}).

Note: collection of $\boldsymbol{\nu}_{\mathrm{X}}$, $\boldsymbol{I}_{\mathrm{X}}$, $\mu_{\perp}$, $|\Delta\mathbf{G}|$ and $\bar{\mathbf{G}}$ requires the user to perform specific calculations at the MECP. Since the MECP is non-stationary point on either of two PES of corresponding electronic states, conventional vibrational analysis will not work. For that, a special Hessian matrix, called the effective Hessian, should be composed. We implemented calculation and diagonalization of the effective Hessian in the ***effhess*** code provided as part of the NAST package. Details of implementation of ***effhess*** are described in Tools.

TST input data:

The input for transition state theory calculations reduces to:

- $\boldsymbol{\nu}_{\mathrm{R}}$ – vibrational frequencies of the reactant, (cm^{-1})
- $\boldsymbol{I}_{\mathrm{R}}$ – principal moments of inertia of the reactant, (amu × $bohr^2$)
- $\boldsymbol{\nu}_{\mathrm{TS}}$ – vibrational frequencies of the transition state, (cm^{-1})
- $\boldsymbol{I}_{\mathrm{TS}}$ – principal moments of inertia of the transition state, (amu × $bohr^2$)
- E_{X} – electronic energy of MECP, (hartree)
- E_{R} – electronic energy of reactant, (hartree)
- E_{P} – electronic energy of product, (hartree) (optional)

The geometry optimization and hessian calculations have to be performed to collect the input data for a NAST run using electronic structure programs (ESP). Popular ESP are GAMESS[21], Molpro[22], CFOUR[23], Dalton[24], Q-Chem[25] and others. At MECP, two hessian calculations are required to obtain spin-specific Hessian matrices, for example, for the singlet-triplet intersection. These matrices are supplied to ***effhess*** along with state-specific gradients at converged MECP geometry. The ***effhess*** tool currently reads the GAMESS and Molpro output files.

References

(1) Lykhin, A. O.; Kaliakin, D. S.; DePolo, G. E.; Kuzubov, A. A.; Varganov, S. A. Nonadiabatic Transition State Theory: Application to Intersystem Crossings in the Active Sites of Metal-Sulfur Proteins. *Int. J. Quantum Chem.* **2016**, *116* (10), 750–761. https://doi.org/10.1002/qua.25124.

(2) Lykhin, A. O.; Varganov, S. A. Intersystem Crossing in Tunneling Regime: T1 → S0 Relaxation in Thiophosgene. *Phys. Chem. Chem. Phys.* **2020**, *22* (10), 5500–5508. https://doi.org/10.1039/c9cp06956a.

(3) Bearpark, M. J.; Robb, M. A.; Bernhard Schlegel, H. A Direct Method for the Location of the Lowest Energy Point on a Potential Surface Crossing. *Chem. Phys. Lett.* **1994**, *223* (3), 269–274. https://doi.org/10.1016/0009-2614(94)00433-1.

(4) Harvey, J. N.; Aschi, M.; Schwarz, H.; Koch, W. The Singlet and Triplet States of Phenyl Cation. A Hybrid Approach for Locating Minimum Energy Crossing Points between Non-Interacting Potential Energy Surfaces. *Theor. Chem. Accounts Theory, Comput. Model.* **1998**, *99* (2), 95–99. https://doi.org/10.1007/s002140050309.

(5) Fernández-Ramos, A.; Ellingson, B. A.; Meana-Pañeda, R.; Marques, J. M. C.; Truhlar, D. G. Symmetry Numbers and Chemical Reaction Rates. *Theor. Chem. Acc.* **2007**, *118* (4), 813–826. https://doi.org/10.1007/s00214-007-0328-0.

(6) Green, N. J. B. *Unimolecular Kinetics Part 1. The Reaction Step*; Elsevier, 2003.

(7) Landau, L. D. No Title. *Phys. Z. Sowjetunion* **1932**, No. 1, 88–98.

(8) Landau, L. D. No Title. *Phys. Z. Sowjetunion* **1932**, *2*, 46–51.

(9) Zener, C. No Title. *Proc. R. Soc. A Math. Phys. Eng. Sci.* **1932**, *137* (696–702).

(10) Stueckelberg, E. C. G. Theory of Inelastic Collisions between Atoms. *Helv. Phys. Acta* **1932**, *5*, 369–422.
(11) Nikitin, E. E. Nonadiabatic Transitions near the Turning Point in Atomic Collisions. *Opt. Spectrosc. (USSR)(English Transl.* **1961**, *11*, 246–248.
(12) Fedorov, D. A.; Lykhin, A. O.; Varganov, S. A. Predicting Intersystem Crossing Rates with AIMS-DFT Molecular Dynamics. *J. Phys. Chem. A* **2018**, *122* (13), 3480–3488.
(13) Delos, J. B. On the Reactions of N 2 with 0. *J. Chem. Phys.* **1973**, *59* (5), 2365–2369.
(14) Dashevskaya, E. I.; Nikitin, E. E. Uniform Airy Approximation for Nonadiabatic Transitions in a Curve-Crossing Weak-Coupling. *Z. Phys. Chem.* **2017**, *232* (3), 311–323.
(15) Zhao, Y.; Mil, G.; Nakamura, H. Evaluation of Canonical and Microcanonical Nonadiabatic Reaction Rate Constants by Using the Zhu – Nakamura Formulas Evaluation of Canonical and Microcanonical Nonadiabatic Reaction Rate Constants by Using the Zhu – Nakamura Formulas. **2012**, *8854* (2004). https://doi.org/10.1063/1.1801971.
(16) Zhao, Y.; Mil'nikov, G.; Nakamura, H. Evaluation of Canonical and Microcanonical Nonadiabatic Reaction Rate Constants by Using the Zhu-Nakamura Formulas. *J. Chem. Phys.* **2004**, *121* (18), 8854–8860. https://doi.org/10.1063/1.1801971.
(17) Melissas, V. S.; Truhlar, D. G.; Garrett, B. C. Optimized Calculations of Reaction Paths and Reaction-Path Functions for Chemical Reactions. *J. Chem. Phys.* **1992**, *96* (8), 5758–5772. https://doi.org/10.1063/1.462674.
(18) Kuki, A. Adiabaticity Factor for Electron Transfer in the Multimode Case: An Energy Velocity Perspective. *J. Phys. Chem.* **1993**, *97*, 13107–13116.
(19) Fedorov, D. G.; Koseki, S.; Schmidt, M. W.; Gordon, M. S. Spin-Orbit Coupling in Molecules: Chemistry beyond the Adiabatic Approximation. *Int. Rev. Phys. Chem.* **2003**, *22* (3), 551–592. https://doi.org/10.1080/0144235032000101743.
(20) Bracewell, R. N. *The Fourier Transform and Its Applications*, 3d ed.; McGraw-Hill, 2000.
(21) Schmidt, M. W.; Baldridge, K. K.; Boatz, J. A.; Elbert, S. T.; Gordon, M. S.; Jensen, J. H.; Koseki, S.; Matsunaga, N.; Nguyen, K. A.; Su, S.; et al. General Atomic and Molecular Electronic Structure System. *J. Comput. Chem.* **1993**, *14* (11), 1347–1363. https://doi.org/10.1002/jcc.540141112.
(22) Werner, H. J.; Knowles, P. J.; Knizia, G.; Manby, F. R.; Schütz, M. Molpro: A General-Purpose Quantum Chemistry Program Package. *Wiley Interdiscip. Rev. Comput. Mol. Sci.* **2012**, *2* (2), 242–253. https://doi.org/10.1002/wcms.82.
(23) Matthews, D. A.; Cheng, L.; Harding, M. E.; Lipparini, F.; Stopkowicz, S.; Jagau, T. C.; Szalay, P. G.; Gauss, J.; Stanton, J. F. Coupled-Cluster Techniques for Computational Chemistry: The CFOUR Program Package. *J. Chem. Phys.* **2020**, *152* (21), 214108. https://doi.org/10.1063/5.0004837.
(24) Aidas, K.; Angeli, C.; Bak, K. L.; Bakken, V.; Bast, R.; Boman, L.; Christiansen, O.; Cimiraglia, R.; Coriani, S.; Dahle, P.; et al. The Dalton Quantum Chemistry Program System. *Wiley Interdiscip. Rev. Comput. Mol. Sci.* **2014**, *4* (3), 269–284. https://doi.org/10.1002/wcms.1172.

(25) Shao, Y.; Gan, Z.; Epifanovsky, E.; Gilbert, A. T. B.; Wormit, M.; Kussmann, J.; Lange, A. W.; Behn, A.; Deng, J.; Feng, X.; et al. Advances in Molecular Quantum Chemistry Contained in the Q-Chem 4 Program Package. *Mol. Phys.* **2015**, *113* (2), 184–215. https://doi.org/10.1080/00268976.2014.952696.
(26) Harvey, J. N.; Aschi, M. Spin-Forbidden Dehydrogenation of Methoxy Cation: A Statistical View. *Phys. Chem. Chem. Phys.* **1999**, *1* (24), 5555–5563. https://doi.org/10.1039/a907723e.
(27) Dubnikova, F.; Lifshitz, A. Isomerization of Propylene Oxide. Quantum Chemical Calculations and Kinetic Modeling. *J. Phys. Chem. A* **2000**, *104* (19), 4489–4496. https://doi.org/10.1021/jp004038+.
(28) Lifshitz, A.; Tamburu, C. Isomerization and Decomposition of Propylene Oxide. Studies with a Single-Pulse Shock Tube. *J. Phys. Chem.* **1994**, *98*, 1161–1170.
(29) Glowacki, D. R.; Liang, C. H.; Morley, C.; Pilling, M. J.; Robertson, S. H. MESMER: An Open-Source Master Equation Solver for Multi-Energy Well Reactions. *J. Phys. Chem. A* **2012**, *116* (38), 9545–9560. https://doi.org/10.1021/jp3051033.
(30) Baer, T.; Hase, W. L. *Unimolecular Reaction Dynamics*; 1996. https://doi.org/10.1093/oso/9780195074949.001.0001.
(31) Hoare, M. R.; Ruijgrok, T. H. W. Inversion of the Partition Function: The First-Order Steepest-Descent Method. *J. Chem. Phys.* **1970**, *52* (1), 113–120. https://doi.org/10.1063/1.1672655.
(32) McGarvey, J. J.; Wilson, J. Photochemical Perturbation and Chemical Relaxation of the Planar - Tetrahedral Equilibrium in a Di(Tertiary Phosphine) Complex of Nickel(II). *J. Am. Chem. Soc.* **1975**, *97* (9), 2531–2532.
(33) Fujiwara, T.; Moule, D. C.; Lim, E. C. Optical-Optical Double Resonance Probe of the Dark State of Thiophosgene in Supersonic Free Jet. *Chem. Phys. Lett.* **2004**, *389* (1–3), 165–170. https://doi.org/10.1016/j.cplett.2004.03.093.
(34) Fujiwara, T.; Lim, E. C. Temporal Characteristics of the S1 and T1 Thiophosgene Cl2 CS in the Gas Phase: Comparison of the T1 Decay with Theoretical Predictions. *J. Chem. Phys.* **2008**, *129* (4), 1–5. https://doi.org/10.1063/1.2963037.
(35) Moule, D. C.; Burling, I. R.; Liu, H.; Lim, E. C. The Cavity Ringdown Spectrum of the Visible Electronic System of Thiophosgene: An Estimation of the Lifetime of the T1(ã 3A2) Triplet State. *J. Chem. Phys.* **1999**, *111* (11), 5027–5037. https://doi.org/10.1063/1.479760.
(36) Rashev, S.; Moule, D. C.; Djambova, S. T. On the T1 → S0 Intersystem Crossing Rate Constant in Thiophosgene. *Chem. Phys. Lett.* **2007**, *441* (1–3), 43–47. https://doi.org/10.1016/j.cplett.2007.04.093.
(37) Miller, J. A.; Klippenstein, S. J. From the Multiple-Well Master Equation to Phenomenological Rate Coefficients: Reactions on a C3H4 Potential Energy Surface. *J. Phys. Chem. A* **2003**, *107* (12), 2680–2692. https://doi.org/10.1063/5.0046438.

3. Program structure

3.1. Input structure

Execution of the NAST package is controlled by the keywords and molecular data read from an input file. As an example, consider modeling kinetics of the spin-forbidden dehydrogenation of triplet methoxy cation:[26]

Example

```
&keys
printmore = .true.                                    ! Print auxiliary data
&end

&inputdata
freX = 671, 1064, 1093, 1301, 1429, 2071, 2855, 2967      ! MECP vib. frequencies
freR = 848, 854, 1122, 1122, 1230, 1239, 2676, 2683, 2685 ! Reactant vib. frequencies
inertX = 12.085, 56.731, 57.962                  ! MECP moments of inertia
inertR = 12.151, 59.527, 59.531                       ! Reactant moments of inertia
enX = 0.022788                                        ! MECP electronic energy
enR = 0                                               ! Reactant energy
maxn = 20000                                 ! Energy integration limit
T1 = 290.0                                            ! Initial temperature
T2 = 300.0                                            ! Final temperature
&end

&probability
redmass = 1.318                                       ! Reduced mass at MECP
soc = 45.7                                            ! SOC at MECP
grad = 0.16575                                        ! Norm of parallel gradient
gradmean = 0.08190                                    ! Geometric mean
&end
```

End of example

The standard input file consists of three data groups, **&keys**, **&inputdata** and **&probability**. The keywords of the **&keys** group specify the calculation type. For example, solution=.true. keyword would simulate reaction kinetics in solution phase (default: .false.).

3.2. Groups and keywords

Given below is the full list of data groups and keywords used by NAST. **Note:** order of data groups in the input file matters. Groups should be given in the following order:

&keys
&inputdata
&external (if extern=.t. in &keys)
&probability (if tst=.f. in &keys)
&reverse (if rev=.t. in &keys)
&split (if sp=.t. in &keys)
&polynomials (if zn=.t. in &keys)

&keys

zpe — Possible values are 0, 1 and 2. ZPE = 0 means no ZPE correction is applied. ZPE = 1 is a regular ZPE correction. ZPE = 2 accounts for turning points below ZPE. (Default ZPE =1).

extern — If .true., reads **&external** group to include external vibrational levels of reactant and/or MECP and/or product. Should be used in case some vibrational mode(s) of a molecule is (are) not described by a harmonic oscillator model. An example is a double well vibrational mode of the lowest triplet state of a thiophosgene molecule ($CSCl_2$). (Default: .false.).

zn — If .true., activates Zhu-Nakamura calculation of the ISC probability. **Note:** Zhu-Nakamura is currently implemented only for **sloped-type** ISC (Section 2.3. NAST equations). **Note:** Zhu-Nakamura requires explicit 1D crossing spin-diabatic potentials to be given in **&polynomials** group described below. **Note:** one way to calculate these potentials is to use our ***ircfit*** code, provided along with NAST. (Default: .false.)

rev — If set .true., additionally invokes calculation of reverse rate constant. See **&reverse** group for more input data. **Note:** Need to define reactant → MECP and product → MECP with direct and reverse reactions, correspondingly, where E (reactant) > E (product). That is, product denotes the lowest energy state.

sp — Calculates the Landau-Zener transition probabilities between individual M_S components of the spin multiplets

in contrast to the average (effective) transition probability (default: false). Should not be used with the **solution** and **tst** set .true.

solution — Turns on calculations in solution phase (default .false.). If .true., the rovibrational densities of states are replaced by vibrational densities.

tst — when set .true., calculates rate constants for traditional Transition State Theory: MECP is replaced with classical Transition State (TS) and the probability of transition is Heaviside step function at energy of TS. The **&probability** group does not need to be provided.

printmore — Controls output flow. If **printmore**=**.t.**, auxiliary data will be printed including all densities of states.

&end

&inputdata

symR
symX — Symmetry numbers of reactant and the MECP. Symmetry number equals to the order of the symmetry group of the molecule. Used to calculate reaction path degeneracy as multiplier of the rate constant (Default 1).

chir — Number of chiral equivalents of the MECP (Default 1).

freR
freX — Fundamental frequencies of reactant and MECP, correspondingly. If external vibrational modes are used (see **&external** below), fundamental frequencies of 'incorrect' vibrational modes of **freR** and/or **freX** should be removed. **Note: freX** comes from the effective Hessian calculations.

inertR
inertX — (I_{xx}, I_{yy}, I_{zz}) rotational moments of inertia.

Important: the **enX** and **enR** keywords below define the absolute (**enX** = -X, **enR** = -Y) or relative (**enX** = -X – (-Y), **enR** = 0) electronic energies for MECP and reactants, respectively. **Note:** the ΔZPE correction to the MECP barrier is calculated and added automatically by the NAST package from vibrational frequencies provided in the input file.

enX	Electronic energy of MECP barrier in hartree. If **rev = .false.** in **&keys**, a good way to set enX is relative to reactant: enX = enX – enR and enR = 0. If **rev = .true.**, better provide absolute value of MECP energy delivered by your electronic structure method of choice.
enR	Energy of reactant. If **enX** is relative to reactant, **enR** should equal zero (see example of input file in 3.1.), which is typical for **rev = .false.** in **&keys**. Otherwise, set absolute energy. In this case enR should be greater than enP (enR > enP) as product should be the lowest energy state.
maxn	Energy integration limit. Set maxn high enough to achieve convergence in canonical rate constants. Our recommendation is to set maxn at least 1.5 larger than the enX barrier.
T1, T2, Tstep	Temperature range [**T1 : Tstep : T2**] for canonical rate constant calculations. Default values are [290 : 1 : 300].

&end

&external

extR, extX, extP	External vibrational levels for reactant, MECP and product, respectively.

&end

3.2.1 External vibrations

Vibrational frequencies in the NAST input file are used to calculate densities of vibrational states. However, some molecular structures have vibrational modes that cannot be described by simple harmonic oscillator (HO) model. Therefore, frequencies of such modes should not be provided in the input file. Instead, vibrational levels of external modes known from experiment or other computational studies should be given, if available. In the NAST package, inclusion of external vibrations can be down using the following syntax:

&keys extern = .true. &end	Set **extern = .true.** to read external vibrational levels in the **&external** group.

&external **extR = 0, 298, 303,..** **&end**	For example, there is one external vibrational mode for reactant, say, described by a double-well potential like in case of thiophosgene.[2] The corresponding vibrational levels are given in **extR**.

The **&probability** group below holds input data to calculate transition. If a classical Transition State Theory run is chosen through **TST = .true.** in **&keys**, then probabilities are replaced with the Heaviside step function and the **&probability** group is not read from the input file. Therefore, a user does not need to provide this group if running a TST job.

&probability

redmass	Reduced mass along the reaction coordinate (RC). Comes from the effective Hessian (EH) calculations.
soc	Spin-Orbit Coupling (SOC) value at the MECP.
grad	$\|\Delta\mathbf{G}\|$, gradient parallel to the RC. Comes from EH calculations.
gradmean	$\bar{\mathbf{G}}$, gradient mean. Comes from EH calculations.

&end

The **&polynomials** group below contains the coefficients of polynomials used to fit 1-D crossing spin-diabatic potentials of two spin states. These coefficients need to be provided to calculate rate constants with the Zhu-Nakamura transition probability. The highest polynomial order supported by NAST is four, i.e. quartic polynomial. Therefore, all five coefficients must be given in the input file even if some are actually zero.

&reverse

symP	symmetry number of product (Default: 1).
freP, inertP, enP	same format as in **&inputdata**

&end

3.2.2 Reverse rate calculations

By default, the NAST package calculates only forward rate constants. The forward direction is defined as the transition from the higher energy spin state (reactant, R) to the

lower energy spin state (product, P). Such calculations require molecular properties only at the reactant minimum and MECP (or TS). In addition, NAST package allows to perform reverse rate calculations via **rev** keyword set **.true.** in **&keys**. To invoke reverse calculation for a TST run, both **rev** and **tst** should be set **.true.** Therefore, rates in forward and backward directions can be calculated in one run. Requesting reverse rate constant calculations requires certain modifications to the input file:

Example

```
&keys ZPE = 1 printmore  = .true rev = .true. &end

&inputdata
freX = 671, 1064, 1093, 1301, 1429, 2071, 2855, 2967
freR = 848, 854, 1122, 1122, 1230, 1239, 2676, 2683, 2685
inertX = 12.085, 56.731, 57.962
inertR = 12.151, 59.527, 59.531
enX = -114.45522
enR = -114.47801
maxn = 20000
T1 = 290.0
T2 = 300.0
&end

&probability
redmass = 1.3188 soc = 45.7
grad = 0.16575 gradmean = 0.08190
&end

&reverse
freP = 1020, 1112, 1246, 1377, 1477, 1663, 3066, 3207, 3566
inertP = 9.036 52.413, 61.449
enP = -114.62007
&end
```

End of example

One could imagine running two independent input files to avoid dealing with extra keywords. There is no problem to run a separate $\mathrm{P} \rightarrow \mathrm{MECP\ (or\ TS)} \rightarrow \mathrm{R}$ Landau-Zener NAST or traditional TST calculation because in both of them the tunneling contribution is neglected. Therefore, ability to run LZ NAST or TST in both directions in one run is implemented for user's convenience. However, there is a strict necessity to run reverse calculation together with the forward one when considering tunneling. With definition of

reactant as higher-energy state and product as lower-energy state, there comes no tunneling (or tunneling with infinite barrier width) in the $E_{\mathrm{R}} - E_{\mathrm{P}}$ energy range for the reverse reaction (Figure 1). Such simultaneous run via **rev=.true.** therefore allows the NAST package to use this information to correct the reverse rate constant for this tunneling range.

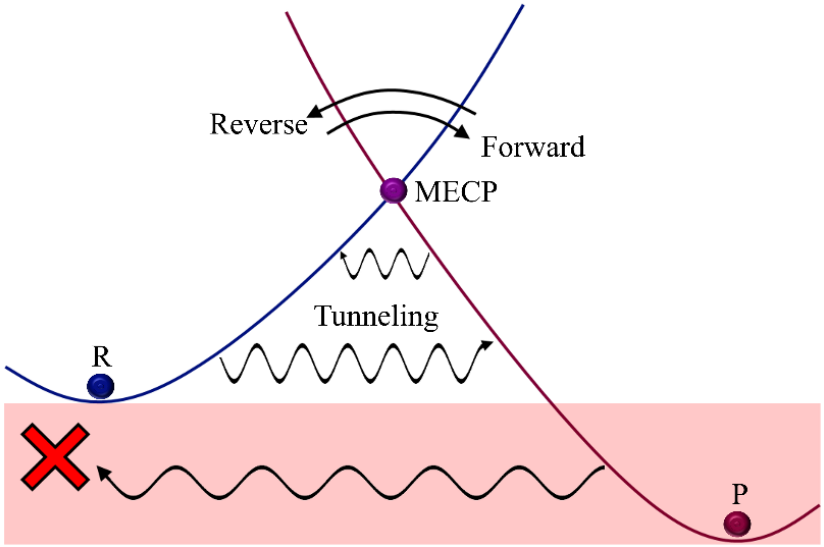

Figure 1. Interstate transitions between two spin states. States are defined according to the $E_{\mathrm{X}} > E_{\mathrm{R}} > E_{\mathrm{P}}$ energy order. Wiggly arrows indicate tunneling contribution to transitions in forward and reverse directions. Arrows above MECP describe classical transition region, where LZ NAST and traditional TST calculations do not depend on direction of a reaction.

Note: A simultaneous run using **rev = .true.** might require a more careful choice of **maxn** energy integration limit in **&inputdata**. The maxn limit is always defined with respect to reactant. For reverse rate calculation, maxn → maxn + $(E_{\mathrm{R}} - E_{\mathrm{P}})$. However, it can appear to be not enough to converge reverse rate constant, if, say, product minimum lies much lower in energy than minimum of reactant. Better try several runs increasing maxn to check convergence or set maxn once to be really large.

Given below are input data, which control calculation of rate constants and transition probabilities between specific M_S components of two spin states. This calculation type is invoked with **sp = .true.** in **&keys**.

&split

mults — Multiplicities of reactant and product, respectively. For example, for a singlet-triplet transition, mults = 1,3.

icp — Number of independent coupling parameters (icp) at the MECP. These are the spin-orbit coupling matrix elements. For example, for a singlet-triplet transition, icp = 2 (see Table 1).

socmat — Independent coupling parameters: they are not complex conjugate of each other, and they are either complex or imaginary numbers. Each number should be given in parenthesis, like (Real part, Imaginary part) and separate parenthesis by comma. For example, for a singlet-triplet transition, socmat = (Re(z), Im(z)), (0, b).

&end

Table 1. Independent coupling parameters (icp) for interstate transitions between states of different spin multiplicities.

Types of transition	Multiplicity of reactant, product	Number of independent coupling parameters (icp)	SOC matrix elements
Singlet-Triplet	1,3	2	z, ib
Doublet-Quartet	2,4	3	z_1, ib, z_2
Triplet-Quintet	3,5	5	$z_1, ib_1, z_2, z_3, ib_2$
Quartet-Sextet	4,6	6	$z_1, ib_1, z_2, z_3, ib_2, z_4$

&polynomials (read if **zn** = **.true.** in **&keys**)

hs4-hs0 — Polynomial coefficients for the potential of reactant, R: R → MECP → P, $E_R > E_P$, where E is an energy at equilibrium geometry. The hs4 coefficient corresponds to the leading order: $f(r) = hs4r^4 + hs3r^3 + \ldots$, where r is 1-D reaction coordinate.

ls4-ls0	Coefficients for product potential.
limitL, limitR	limitL and limitR are the left and right limits along r. limitR must be greater than limitL. limitL should be chosen at the reactant minimum (minimum of R in R → MECP → P). The choice of limitR depends on the intersection type. For the sloped intersection, limitR should be chosen so that energy of reactant potential at this point is well above MECP to ensure convergence: E(limitR) = f(hs,limitR) >> E_{MECP}, where f is polynomial describing the reactant potential. **Note:** Detailed explanation of how to obtain 1-D crossing potentials using the ***ircfit*** tool is given in Section 6.2.

&end

4. Navigation through output files

4.1. nast.out

The main output file generated by NAST is *nast.out*. This file contains the canonical rate constants and velocity-averaged transition probabilities. An example of *nast.out* is given below:

Example of nast.out ($T_1 \rightarrow S_0$ relaxation in thiophosgene in the tunneling regime)

```
-------------------------------------------------------
          NAST control parameters and related data

     zpe = 2   sp = F   zn = T   solution = F
   tst = F   printmore = T   rev = F   extern = T
-------------------------------------------------------
zpe = 2: ZPE correction scheme II (accounts for turning points below ZPE).
 Electronic barrier from reactant to MECP is 3185 cm-1
 ZPE of reactants = 0.00 cm-1
 ZPE of MECP = 0.00 cm-1
 ZPE-corrected MECP energy bin = 3186 cm-1
```

Canonical rate constant, k(T)

T (K)	Landau-Zener	Weak Coupling	Zhu-Nakamura
296.0	0.00E+00	2.04E+08	9.00E+05
297.0	0.00E+00	2.05E+08	9.06E+05

Landau-Zener and Weak Coupling double passage velocity-averaged probabilities of transition, p(T)
Calculated using Maxwell-Boltzmann (MB) and Kuki (K) distributions

T (K)	Landau-Zener MB	Landau-Zener K	Weak Coupling MB	WC K
296.0	0.6823	0.4628	0.0142	0.0001
297.0	0.6819	0.4623	0.0142	0.0001

End of example

4.2. energy_rates.out

This file contains the microcanonical rate constants calculated using the LZ, WC and ZN (optional) probability formulas.

4.3. energy_probabilities.out

This file contains the microcanonical transition probabilities calculated using the LZ, WC and ZN (optional) formulae.

4.4. Densities of states (optional, if printmore = .true. in &keys)

There is a group of output files containing the rotational, vibrational and rovibrational densities of states at reactant (dos_reactant.out), MECP (dos_mecp.out), transition state TS (dos_ts.out) if **tst** is set **.true.** in **&keys**, and dos_product.out if **rev** is set **.true.** in **&keys**. In addition, the densities of turning points, calculated using the molecular properties at MECP, are stored in dos_tp.out.

4.5. split_probabilities.out (optional, if sp = .true. in &keys)

This file contains the microcanonical probabilities of transitions between the M_S components of two spin states using the LZ formula.

4.6. split_energy_rates.out (optional, if sp = .true. in &keys)

This file contains the microcanonical rate constants of transitions between the M_S components of two spin states.

5. Examples

We first start with examples for classical transition state theory, TST, as a limiting and simplified case of NAST. The TST examples we discuss in Sections 5.1 and 5.2 below. NAST examples are covered in Sections 5.3 – 5.7. Examples 5.5 and 5.6 show application of the Zhu-Nakamura approach to calculate transition probabilities.

5.1. Example 1. TST case study: Isomerization of Propylene Oxide to Acetone and Propanal

This example demonstrates how the NAST package can be used to calculate the reaction rates for single-state adiabatic reactions using the traditional TST. We consider the isomerization of propylene oxide to acetone and propanal, following the original theoretical work of Dubnikova and Lifshitz[27]. For each isomerization reaction, four canonical TST rate constants were compared: i) predicted by the NAST package, ii) calculated analytically using equation 2.27, iii) calculated analytically using equation 5.1 below[27] and iv) experimental [28],

$$k(T) = \sigma \frac{k_B T}{h} e^{-\Delta S^{\#}/R} e^{-\Delta H^{\#}/RT}, \tag{5.1}$$

where R is the universal gas constant; $\Delta S^{\#}$and $\Delta H^{\#}$ are the entropy and enthalpy of activation, respectively. Because for a unimolecular reaction, $\Delta H^{\#} = E_{\mathrm{TS}} + \Delta\mathrm{ZPE}$, the activation enthalpy is equal to the ZPE-corrected electronic barrier between transition state and reactant. The input data for NAST were obtained using the B3LYP geometry optimization and Hessian calculations in GAMESS, and the single-point CCSD(T) energy calculations in Molpro. The cc-pVDZ basis set was used in all calculations. The partition functions Q_{TS} and Q_{R} used in Eq. 25 were taken as calculated by GAMESS. In equation 5.1, the original data from Table 1 of Dubnikova and Lifshitz [27] was used. The energy profiles for two isomerization reactions are shown in Figure 5.1.

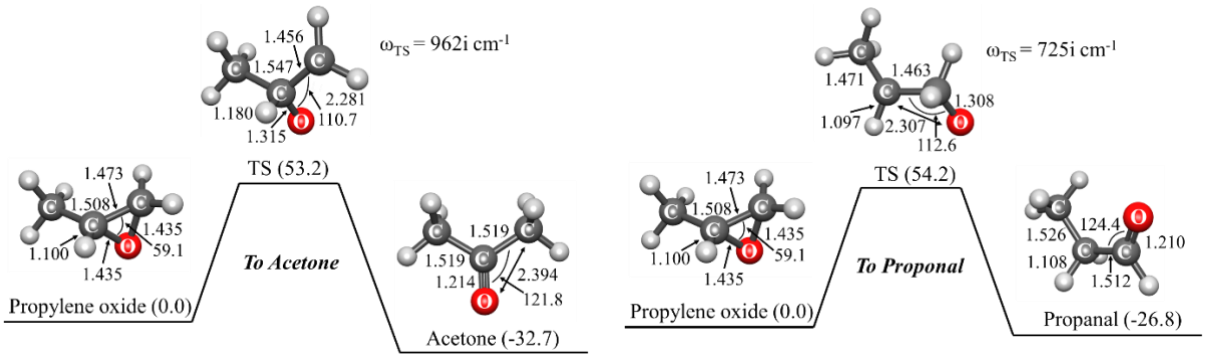

Figure 5.1. Energies and structural parameters for the isomerization reactions of propylene oxide to acetone (left) and propanal (right). The relative CCSD(T) energies (kcal·mol^{-1}) in parenthesis are corrected with the $\Delta ZPE = ZPE_{\mathrm{X}} - ZPE_{\mathrm{R}}$ calculated with B3LYP. Bond lengths and angles are given in Å and degrees, respectively.

The NAST input file and the main parts of output file are shown below.

Input file

```
&keys zpe = 1 tst = .true. &end ! Traditional TST calculation set true.

&inputdata
freX = 263, 294, 374, 580, 729, 871, 886, 958, 999, 1081, 1118, 1241, 1283, 1357, 1434, 1452, 1471, 2296, 3026,
3092, 3118, ,3142, 3238
freR = 240, 370, 416, 773, 848, 903, 974, 102, 1117, 1136, 1153, 1173, 1277, 1381, 1423, 1451, 1471, 1515, 3025,
3059, 3076, 3098, 3117, 3153
inertX = 170.850, 217.264, 351.144 ! Moments of inertia for TS/MECP
inertR = 100.305, 272.514, 305.514 ! Moments of inertia for reactant
enX = 0.09129754 ! Electronic energy of TS in hartree. Program will add ΔZPE
enR = 0.0        ! Energy of reactant in hartree
maxn = 30000     ! Maximum energy bin: integration limit in cm-1
T1 = 1000        ! Initial temperature in K for canonical rate calculation
&end
```

Main parts of the output file

```
  ********************************************************
  ~~~~~~~ NAST: Nonadiabatic Statistical Theory ~~~~~~~~
          ~~~~~ v. 2021.1 ~~~~~
  ********************************************************
----------------------------------------------------------
NAST control parameters and related data

zpe = 1   sp = F   zn = F   solution = F
tst = T   printmore = F   rev = F   extern = F
----------------------------------------------------------

zpe = 1: ZPE correction scheme I (eliminates turning points below ZPE).
Electronic barrier from reactant to MECP is  20037 cm-1
ZPE of reactants =  18586 cm-1
ZPE of MECP =  17150 cm-1
ZPE-corrected MECP energy bin =  18602 cm-1
```

```
 ----------------------------------------------------------
        Start NAST calculation
 ----------------------------------------------------------

 1. Calculating densities of states

.....vibrational.
.....rotational.
.....rovibrational.

Calculating microcanonical TST rate constant.
..... Done.

(The forward rate constant k(E) is multiplied by reaction path degeneracy equal to 1)

       Canonical rate constant, k(T)

  T(K)   TST rate constant

 1000.0      6.78E+01

Total CPU time =  10.35
NAST terminated now.
```

Comparison of results with original work and canonical TST rate constant. Table 5.1 shows the calculated and experimental rate constants for the isomerization of propylene oxide to acetone and propanal. The factor of two difference between the acetone rate constants calculated with two analytical expressions can be explained by a 1.0 kcal·mol^{-1} discrepancy in the TS barrier (using the same barrier height of 53.2 kcal·mol^{-1} in both analytical expressions reduces this difference to 18%). The difference between the NAST rate constant (67.8 s^{-1}) and the analytical constant obtained with equation 5.1 (101.0 s^{-1}) could be due to the accuracy of the numerical integration in NAST. Similar differences in the reaction rates calculated with different methods are observed for the isomerization to propanal. All calculated rate constants are in reasonable agreement with the experimental values for both isomerization reactions.

Table 5.1. Canonical TST rate constants for isomerization of propylene oxide to acetone and propanal at T=1000 K.

Product	Source	E_{TS}, kcal·mol^{-1}	k_{1000}, s^{-1}
Acetone	NAST	53.2	67.8
	Analytical, equation 5.1[a]	54.2	50.2
	Analytical, equation 2.27	53.2	101.0
	Experiment[b]	-	30.0
Propanal	NAST	54.2	43.0
	Analytical, equation 5.1[a]	54.4	69.6
	Analytical, equation 2.27	54.2	88.6
	Experiment[b]	-	90.0

[a] Ref. [27].

[b] Experimental values are estimated from the log(k) vs. T plots in Ref. [28].

Analysis of convergence and execution time. Here we bring example of convergence in rate constant calculations and CPU time vs. the maxn integration limit (Figure 5.2). The calculations were run on a single core on a cluster machine, Rocks 7.0/CentOS 7.0 (Core), x86_64, Intel(R) Xeon(R) CPU E5630 @ 2.53GHz.

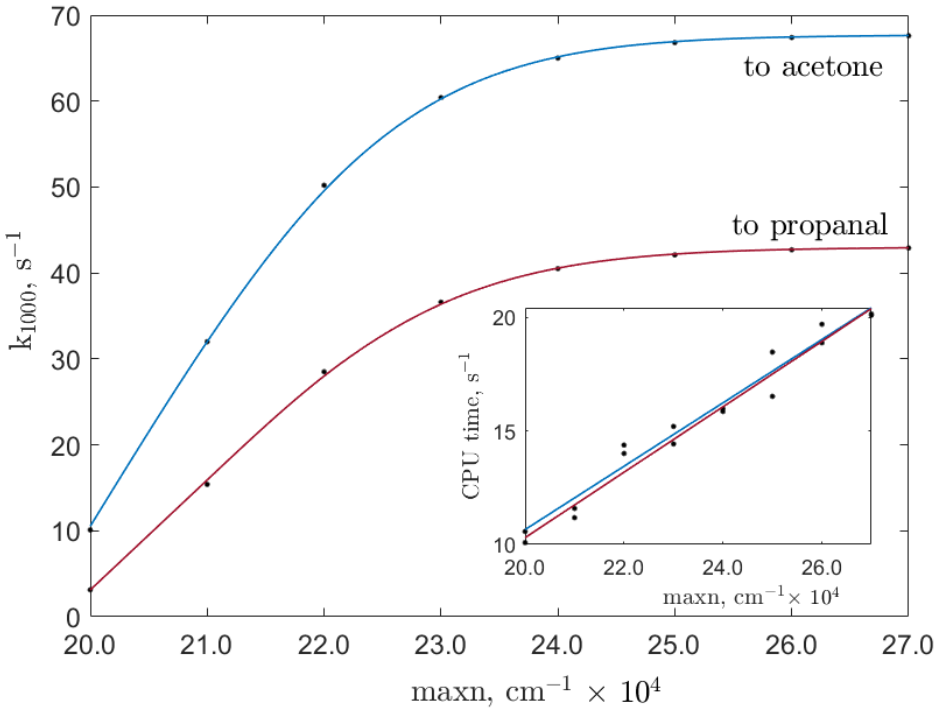

Figure 5.2. Convergence in rate constant calculations vs. maxn integration limit in isomerization of propylene oxide to acetone and to propanal. The transition state (TS) energy for isomerization to acetone was 18 602 cm^{-1}, and to propanal – 18 969 cm^{-1}.

For acetone, the zero-point-energy-included electronic TS barrier was 18 602 cm^{-1} with respect to reactant as calculated at the CCSD(T)/cc-pVDZ level of theory. Therefore, we concluded fast convergence since the rate plateau is reached already at around 26 000 cm^{-1}. The calculation time approximately follows linear growth. The same trend in convergence and CPU time growth is found for isomerization to propanal.

References

(27) Dubnikova, F.; Lifshitz, A. Isomerization of Propylene Oxide. Quantum Chemical Calculations and Kinetic Modeling. *J. Phys. Chem. A* **2000**, *104* (19), 4489–4496. https://doi.org/10.1021/jp004038+.

(28) Lifshitz, A.; Tamburu, C. Isomerization and Decomposition of Propylene Oxide. Studies with a Single-Pulse Shock Tube. *J. Phys. Chem.* **1994**, *98*, 1161–1170.

5.2. Example 2. TST case study: Cis-trans isomerization in but-2-ene

In this example, we compare the canonical rate constants of adiabatic TST reaction of cis-to-trans and trans-to-cis isomerization in but-2-ene calculated with the NAST and MESMER packages.[29] The NAST input data were taken from a MESMER input file (cis_to_trans_But-2-ene.xml). In the MESMER input file, the relative energies of reactant, TS and product are corrected to ZPE, while in the NAST input file, electronic energies should be provided, and the ZPE correction will be added automatically. Thus, in the NAST input file we subtracted the ZPE correction added by MESMER to get electronic barriers. Given below are input and output files for cis-to-trans isomerization.

Input file

```
$keys zpe = 1 printmore = .true. tst=.true. &end

&inputdata
freX=131, 131, 304, 304, 304, 1000, 1000, 1000, 1000, 1000, 1000, 1000, 1340, 1340, 1340, 1452, 1452, 1452,
1452, 1452, 1672, 2976, 2976, 2976, 2976, 2976, 2976, 2976, 2976
inertX=109.86829, 396.10409, 396.10409
freR=258, 290, 290, 396, 575, 673, 873, 950, 970, 1009, 1037, 1050, 1134, 1261, 1380, 1387, 1408, 1464, 1464,
1464, 1464, 1670, 2878, 2935, 2950, 2988, 2988, 2988, 3036, 3050
inertR=109.86829, 354.16366, 442.70456
enX = 0.102777
enR = 0.0
maxn=40000
T1=100
Tstep=100
T2=2000
&end
```

Main parts of the output file

```
  *******************************************************
  ~~~~~~~ NAST: Nonadiabatic Statistical Theory ~~~~~~~~
          ~~~~~ v. 2021.1 ~~~~~
  *******************************************************
-----------------------------------------------------------
NAST control parameters and related data

zpe = 1   sp = F   zn = F   solution = F
tst = T   printmore = T   rev = F   extern = F
-----------------------------------------------------------

zpe = 1: ZPE correction scheme I (eliminates turning points below ZPE).
Electronic barrier from reactant to MECP is 22556 cm-1
ZPE of reactants =  23140 cm-1
ZPE of MECP =  22467 cm-1
ZPE-corrected MECP energy bin =  21884 cm-1
 ---------------------------------------------------------
       Start NAST calculation
 ---------------------------------------------------------
```

```
 1. Calculating densities of states

.....vibrational.
.....rotational.
.....rovibrational.

Calculating microcanonical TST rate constant.
..... Done.

(The forward rate constant k(E) is multiplied by reaction path degeneracy equal to 1)

      Canonical rate constant, k(T)

  T(K)   TST rate constant

 100.0   5.02-125
 200.0   2.95E-56
 500.0   3.45E-15
 600.0   1.04E-10
    ...
1800.0   2.47E+04
1900.0   5.54E+04
2000.0   1.14E+05

Total CPU time =   6.66
NAST terminated now.
```

Comparison of the NAST rate constants with those of MESMER are given in Table 5.2 in the temperature range from 100 to 2000 K. In NAST, we set the maxn value to 40 000 cm^{-1} to ensure convergence in canonical rate constants. Similarly, in MESMER, we set temperature of the He gas bath to 2500 K.

Table 5.2. Canonical rate constants for cis-trans and trans-cis isomerization in but-2-ene. Relative difference between the NAST and MESMER values is defined as $(k_{NAST}-k_{MESMER})/k_{MESMER}$.

	k(cis-trans), s^{-1}			k(trans-cis), s^{-1}		
T, K	NAST	MESMER	Relative difference	NAST	MESMER	Relative difference
100	5.02×10^{-125}	8.68×10^{-125}	-0.42	3.47×10^{-127}	6.52×10^{-127}	-0.47
200	3.04×10^{-56}	4.68×10^{-56}	-0.35	2.25×10^{-57}	3.14×10^{-57}	-0.28
300	2.89×10^{-33}	5.44×10^{-33}	-0.47	4.82×10^{-34}	7.07×10^{-34}	-0.32
400	9.32×10^{-22}	2.07×10^{-21}	-0.55	2.38×10^{-22}	3.66×10^{-22}	-0.35
500	7.72×10^{-15}	1.92×10^{-14}	-0.60	2.58×10^{-15}	4.05×10^{-15}	-0.36
600	3.24×10^{-10}	8.61×10^{-10}	-0.62	1.30×10^{-10}	2.04×10^{-10}	-0.36
700	6.64×10^{-07}	1.83×10^{-06}	-0.64	3.03×10^{-07}	4.70×10^{-07}	-0.36
800	2.05×10^{-04}	5.78×10^{-04}	-0.65	1.04×10^{-04}	1.57×10^{-04}	-0.34
900	1.80×10^{-02}	5.09×10^{-02}	-0.65	9.82×10^{-03}	1.45×10^{-02}	-0.32
1000	6.50×10^{-1}	1.83	-0.64	3.78×10^{-1}	5.39×10^{-1}	-0.30

1100	1.23×10^{1}	3.40×10^{1}	-0.64	7.57	1.03×10^{1}	-0.27
1200	1.45×10^{2}	3.81×10^{2}	-0.62	9.26×10^{1}	1.18×10^{2}	-0.22
1300	1.17×10^{3}	2.84×10^{3}	-0.59	7.76×10^{2}	8.99×10^{2}	-0.14
1400	7.04×10^{3}	1.51×10^{4}	-0.53	4.82×10^{3}	4.85×10^{3}	-0.01
1500	3.35×10^{4}	6.03×10^{4}	-0.44	2.36×10^{4}	1.97×10^{4}	0.20
1600	1.32×10^{5}	1.90×10^{5}	-0.31	9.52×10^{4}	6.27×10^{4}	0.52
1700	4.44×10^{5}	4.88×10^{5}	-0.09	3.27×10^{5}	1.63×10^{5}	1.01
1800	1.31×10^{6}	1.06×10^{6}	0.24	9.81×10^{5}	3.56×10^{5}	1.76
1900	3.45×10^{6}	1.99×10^{6}	0.73	2.63×10^{6}	6.75×10^{5}	2.90
2000	8.28×10^{6}	3.32×10^{6}	1.49	6.41×10^{6}	$1.14\times+10^{6}$	4.62

We observed close agreement between calculated canonical rate constants in NAST and MESMER at all temperatures. We recommend a user to set the maxn value to be at least 1.5 as large as the energy gap between the reactant and transition state to ensure convergence in canonical rate constants.

References

(29) Glowacki, D. R.; Liang, C. H.; Morley, C.; Pilling, M. J.; Robertson, S. H. MESMER: An Open-Source Master Equation Solver for Multi-Energy Well Reactions. *J. Phys. Chem. A* **2012**, *116* (38), 9545–9560. https://doi.org/10.1021/jp3051033.

5.3. Example 3. Dehydrogenation of the triplet methoxy cation, CH_3O^+

The spin-forbidden dehydrogenation of the triplet methoxy cation was studied by Harvey and Aschi.[26] The dehydrogenation reaction mechanism is shown below in Figure 5.3 and in Figure 2 of the original paper:

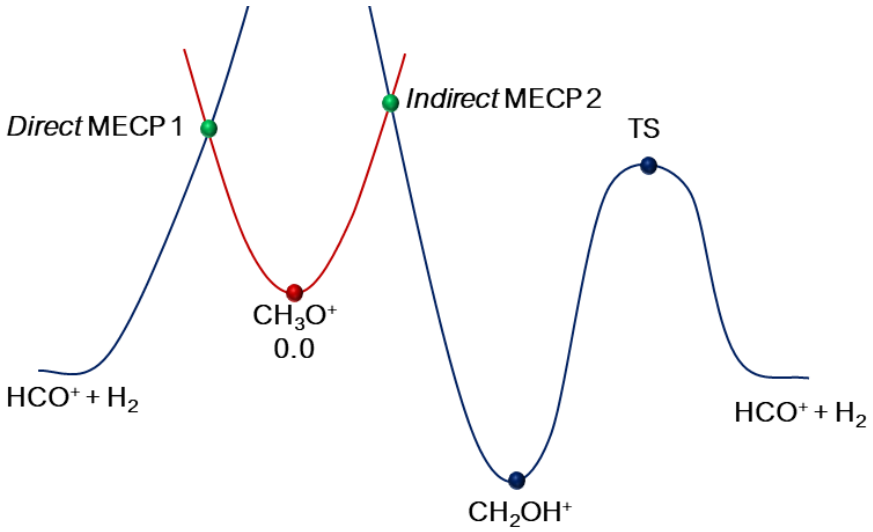

Figure 5.3. Reaction channels of the spin-forbidden dehydrogenation of triplet CH_3O^+.

As shown by Harvey, the dehydrogenation can proceed through two reaction channels, either through states crossing at direct MECP 1 located on the left from $^3CH_3O^+$ reactant minimum, or through indirect MECP 2. In this test example, we consider only interstate transitions happening through MECP 2. The NAST input data were collected at the CCSD(T)/cc-pVTZ level of theory. The electronic MECP barrier was found to be 15.0 kcal mol^{-1}. Our SA-MCQDPT2 calculated SOC value of 64 cm^{-1} is different from the 45.7 cm^{-1} value of Harvey and Aschi, where the latter was derived from FOCI wavefunction and one-electron SOC operator. In this example, Harvey and Aschi's SOC value is used for clearer comparison. The rest of parameters are taken from our calculations. Given below are the corresponding NAST input and output files. These are followed by microcanonical rate constants calculated using the LZ and WC transition probability formulas plotted in Figure 5.4.

Input file

```
$keys zpe = 1 printmore = .true. &end

&inputdata
freX = 671, 1064, 1093, 1301, 1429, 2071, 2855, 2967
inertX = 12.085, 56.731, 57.962
freR = 848, 854, 1122, 1122, 1230, 1239, 2676, 2683, 2685
inertR = 12.151, 59.527, 59.531
enX = 0.022788
enR = 0.0
maxn=20000
T1=290.0
T2=300.0
&end

&probability
redmass = 1.3188
soc = 45.7
grad = 0.16576
gradmean = 0.08190
&end
```

Main parts of the output file

```
  ******************************************************
  ~~~~~~~ NAST: Nonadiabatic Statistical Theory ~~~~~~~~
          ~~~~~ v. 2021.1 ~~~~~
  ******************************************************
----------------------------------------------------------
NAST control parameters and related data
zpe = 1   sp = F   zn = F   solution = F
tst = F   printmore = T   rev = F   extern = F
```

```
-----------------------------------------------------------
zpe = 1: ZPE correction scheme I (eliminates turning points below ZPE).
Electronic barrier from reactant to MECP is 5001 cm-1
ZPE of reactants = 7229 cm-1
ZPE of MECP = 6726 cm-1
ZPE-corrected MECP energy bin = 4499 cm-1

 ----------------------------------------------------------
        Start NAST calculation
 ----------------------------------------------------------

  1. Calculating densities of states

.....vibrational.
.....rotational.
.....rovibrational.

  2. Calculating microcanonical probabilities

    LZ formula is valid at energies much greater than 6031 cm-1.

.....Landau-Zener

Warning! Rate calculations using transition probabilities that account
for quantum tunneling should be run with caution.
Make sure that in a reaction studied, reactant lies higher in energy than product.
Otherwise, there will be a region of unphysical tunneling, which should be excluded.
If this is the case, run a reverse (rev = .true.) calculation. This will allow NAST to prevent
unphysical tunneling. Details on reverse rate calculations can be found in the NAST package manual.

.....Weak Coupling

  3. Calculating microcanonical NAST rate constant
   (The forward rate constant k(E) is multiplied by reaction path degeneracy equal to 1).


       Canonical rate constant, k(T)

   T(K)  Landau-Zener  Weak Coupling
    296.0   1.14E+01     5.25E+06
    297.0   1.23E+01     5.28E+06
    298.0   1.32E+01     5.31E+06

 Total CPU time = 10.11
 NAST terminated now.
```

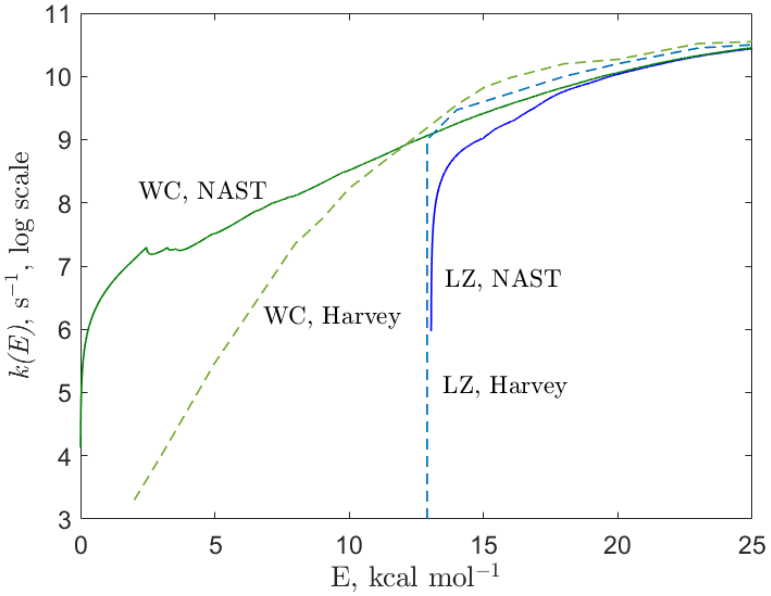

Figure 5.4. Microcanonical rate constants of the spin-forbidden dehydrogenation of CH_3O^+, calculated using the Landau-Zener (LZ, blue) and Weak Coupling (WC, green) probability formulas.

At low energies, there are two prominent effects: i) humps in the NAST predicted rate constants at energies around 2.5 kcal mol^{-1} and ii) around two orders of magnitude difference between rate constant values predicted by NAST and those of Harvey and Aschi. The first effect can be explained by low density of rovibrational states of reactant and MECP at low energies. At higher energies, more rovibrational states are accessible and therefore, the rovibrational density of states becomes a smoother function of energy. This trend is illustrated in Figure 5.5 below by plotting the $\rho_X(E)/\rho_R(E)$ ratio of rovibrational densities of states at MECP and reactant:

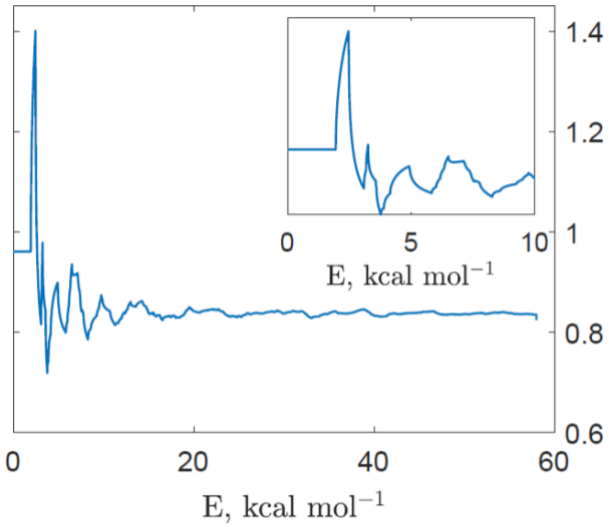

Figure 5.5. Ratio of densities of rovibrational states at MECP and reactant as function of the internal energy E, kcal mol^{-1}.

According to an inset plot in Figure 5.5, the most prominent humps appear at E equal to 2.4, 3.2, and 4.8, respectively. These humps are due to population of few first low-frequency vibrational levels of reactant. Specifically, the first hump at around 2.4 kcal mol^{-1} corresponds to two vibrational modes, 848 cm^{-1} (2.42 kcal mol^{-1}) and 854 cm^{-1} (2.44 kcal mol^{-1}). The next hump at around 3.2 kcal mol^{-1} corresponds to doubly degenerate mode, 1122 cm^{-1} (3.21 kcal mol^{-1}). Finally, the hump at around 4.8 kcal mol^{-1} comes from the first overtones of the 848 cm^{-1} and 854 cm^{-1} modes: 848 cm^{-1} × 2 = 1696 cm^{-1} (4.85 kcal mol^{-1}) and 854 cm^{-1} × 2 = 1708 cm^{-1} (4.88 kcal mol^{-1}). Note that humps reduce in magnitude at higher energies (Figure 5.5). This is due to convolution of larger densities of states.

The second effect clear in Figure 5.5 is around two orders of magnitude difference between rate constant values predicted by NAST and Harvey at low energies. We believe it is due to different approaches used in NAST and Harvey and Aschi to calculate rovibrational densities of states. In the NAST package, we use the direct counting algorithm for vibrational densities of states, classical assymetric top model for rotational densities and calculate convolution integral to obtain ultimate rovibrational densities of states. On the other hand, Harvey and Aschi's approach is different. Starting with the analytical expression for the rovibrational partition function, $Q = Q_{\mathrm{rot}}Q_{\mathrm{vib}}$ the density of the rovibrational states can be obtained via the inverse Laplace transform[30]:

$$\rho(E) = \frac{1}{2\pi i}\int_{c-i\infty}^{c+i\infty} Q(\beta)e^{\beta E}d\beta, \qquad (5.2)$$

where Q is the rovibrational partition function and $\beta = 1/k_B T$. One way to solve the inverse Laplace integral is using the steepest descent method.[31] It is important to know that the rovibrational density $\rho(E)$, calculated in equation 5.2, is a smooth function of E, whereas the real density, due to discreate vibrational levels, is rather unsmooth at low energies. Since NAST calculates $\rho_{\mathrm{vib}}(E)$ using the direct counting algorithm, the resulting vibrational density represents a series of delta functions, whereas calculated in equation 5.2, $\rho_{\mathrm{vib}}(E)$ is non-zero at any E. Obviously, it has great effect on convolution.

References

(26) Harvey, J. N.; Aschi, M. Spin-Forbidden Dehydrogenation of Methoxy Cation: A Statistical View. *Phys. Chem. Chem. Phys.* **1999**, *1* (24), 5555–5563. https://doi.org/10.1039/a907723e.

(30) Baer, T.; Hase, W. L. *Unimolecular Reaction Dynamics*; 1996. https://doi.org/10.1093/oso/9780195074949.001.0001.

(31) Hoare, M. R.; Ruijgrok, T. H. W. Inversion of the Partition Function: The First-Order Steepest-Descent Method. *J. Chem. Phys.* **1970**, *52* (1), 113–120.

https://doi.org/10.1063/1.1672655.

5.4. Example 4. Spin-forbidden izomerization of dichloro-1,3-bis(diphelylophosphino)propanenickel(II)

This is an example of the forward and reverse rate constants calculation in a single NAST run. In addition it demonstrates how the rate constants between individual M_S components of two spin states are calculated. The interconversion between the singlet (planar) and triplet (tetrahedral) isomers of Ni(dpp)Cl_2 complex (dpp – 1,3-bis(diphenylphosphino)propane) has been studied in acetonitrile.[32] To reduce the computational cost, the phenyl groups were replaced by methyl groups (Figure 5.6). The optimized geometries and Hessians for singlet, triplet and MECP structures were obtained with the M11-L density functional, implicit solvation model and def2-TZVP basis set, as implemented in GAMESS. The SOC value of 135 cm^{-1} was calculated with the multiconfigurational quasi-degenerate perturbation theory (MCQDPT2) using the CASSCF(2e, 4o) wavefunction averaged over the lowest energy singlet and triplet states electronic states and the same basis set. The corresponding input files are included in SI. The forward ($S \rightarrow T$) rate constant calculated using the WC transition probability at 296 K (4.96×10^6 s^{-1}) agrees with the experimental value of 4.5×10^5 s^{-1}. However, the reverse ($T \rightarrow S$) rate constants predicted to be 3.50×10^2 s^{-1} is significantly smaller than the experimental values 6.0×10^5 s^{-1}, which could indicate that the barrier for the reverse reaction is overestimated due to the low-level of electronic structure calculations and the reduced model size. The NAST input and output files are given below.

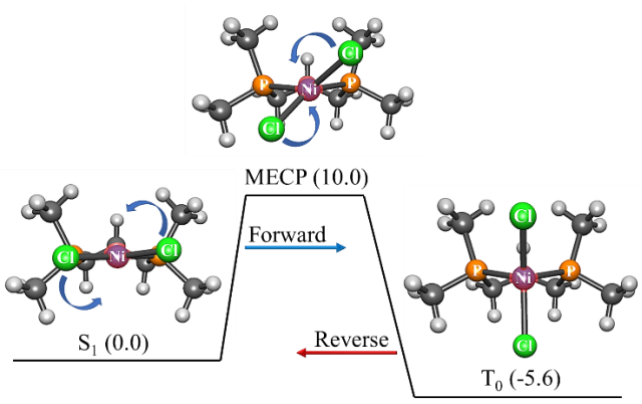

Figure 5.6. Reaction path of singlet-triplet isomerization of the Ni(dpp)Cl_2 model from square-planar to tetragonal geometry. The angles between the Cl-Ni-Cl and P-Ni-P planes are 6°, 42° and 90° for the singlet, MECP and triplet geometries, respectively. The benzene rings of Ni(dpp)Cl_2 are replaced with the methyl groups.

Input file

```
$keys zpe = 1 printmore = .true. rev = .true. solution=.t. &end

&inputdata
freX=44, 64, 90, 94, 120, 130, 146, 155, 168, 184, 192, 197, 201, 206, 219, 226, 233, 253, 262, 270, 319, 325, 352,
371, 453, 638, 680, 720, 743, 751, 762, 768, 793, 813, 826, 842, 865, 902, 911, 944, 953, 954, 1003, 1080, 1116,
1178, 1257, 1285, 1289, 1292, 1303, 1305, 1329, 1378, 1387, 1391, 1395, 1398, 1402, 1404, 1409, 1412, 1421, 1424,
1454, 2983, 2986, 2989, 2990, 2996, 2999, 3000, 3059, 3063, 3066, 3117, 3123, 3127, 3128, 3130, 3142, 3143,
3151
inertX=3509.61929 3642.53089 5640.84788
freR=40 91, 106, 123, 152, 160, 172, 179, 193, 206, 207, 213, 215, 224, 225, 239, 241, 269, 280, 308, 325, 335,
345, 408, 420, 467, 659, 684, 733, 738, 760, 769, 774, 817, 840, 846, 861, 877, 911, 924, 948, 952, 963, 1010,
1088, 1116, 1179, 1263, 1289, 1293, 1294, 1306, 1315, 1328, 1377, 1392, 1394, 1403, 1405, 1407, 1409, 1411, 1421,
1425, 1430, 1458, 2984, 2991, 2992, 2998, 3000, 3001, 3005, 3060, 3070, 3071, 3125, 3126, 3127, 3131, 3148,
3150, 3163, 3164
inertR=3203.70539, 3475.30910, 5655.32379
enX = -3389.355567
enR = -3389.371528
maxn=10000
T1 = 290.0
T2 = 300.0
&end

&probability
redmass=5.05674
soc=135.0
grad=0.046067
gradmean=0.022625
&end

&reverse
freP=32, 47, 57, 72, 80, 82, 126, 140, 156, 169, 173, 179, 186, 203, 205, 215, 221, 228, 245, 252, 279, 314, 315,
359, 363, 444, 647, 677, 733, 742, 745, 766, 771, 806, 819, 828, 842, 864, 905, 907, 941, 951, 956, 1007, 1083,
1123, 1194, 1261, 1289, 1295, 1299, 1304, 1317, 1333, 1368, 1386, 1393, 1394, 1397, 1400, 1404, 1408, 1412, 1415,
1419, 1450, 2980, 2982, 2987, 2993, 2995, 2996, 2997, 3056, 3059, 3063, 3121, 3123, 3122, 3124, 3131, 3133,
3136, 3137
inertP=3614.38309, 4076.66807, 4552.08660
enP = -3389.377261
&end

&split
mults = 1,3
icp = 2
socmat = (-68.98,-63.83),(0,21.32)
&end
```

Main parts of the output file

```
 ********************************************************
 ~~~~~~~ NAST: Nonadiabatic Statistical Theory ~~~~~~~~
          ~~~~~ v. 2021.1 ~~~~~
 ********************************************************
------------------------------------------------------------
   NAST control parameters and related data
```

```
  zpe = 1   sp = F   zn = F   solution = T
  tst = F   printmore = T   rev = T   extern = F
 ---------------------------------------------------------

 zpe = 1: ZPE correction scheme I (eliminates turning points below ZPE).
 Electronic barrier from reactant to MECP is  3505 cm-1
 ZPE of reactants =  52954 cm-1
 ZPE of MECP =  52319 cm-1
 ZPE-corrected MECP energy bin =  2871 cm-1
 ZPE of product is  52260 cm-1.
 Gap between reactant and product is 1951 cm-1.

 ---------------------------------------------------------
        Start NAST calculation
 ---------------------------------------------------------

  1. Calculating densities of states

 ......vibrational.
 ........rotational.
 .........rovibrational.

  2. Calculating microcanonical probabilities

    LZ formula is valid at energies much greater than 3285 cm-1.

 .........Landau-Zener

 Warning! Rate calculations using transition probabilities that account
 for quantum tunneling should be run with caution.
 Make sure that in a reaction studied, reactant lies higher in energy than product.
 Otherwise, there will be a region of unphysical tunneling, which should be excluded.
 If this is the case, run a reverse (rev = .true.) calculation. This will allow NAST to prevent
 unphysical tunneling. Details on reverse rate calculations can be found in the NAST package manual.
 ..........Weak Coupling

  3. Calculating microcanonical NAST rate constant
    (The forward rate constant k(E) is multiplied by reaction path degeneracy equal to 1 ).


        Canonical rate constant, k(T)

   T(K)  Landau-Zener  Weak Coupling
    296.0  1.76E+06     4.96E+06
    297.0  1.85E+06     5.17E+06

 Landau-Zener (LZ) and Weak Coupling (WC) double passage velocity-averaged
                probabilities of transition, p(T)
       Calculated using Maxwell-Boltzmann (MB) and Kuki (K)
                energy distributions

    T(K)   LZ MB    LZ K    WC MB    WC K

    296.0  0.5230   0.3033   0.0137   0.0001
```

```
  297.0  0.5226   0.3029   0.0137   0.0001

Calculating product densities of states.

.....vibrational.
.....product rotational.
.....product rovibrational.

   Reverse LZ probability is valid at energies much greater than 5236 cm-1.
.....Weak Coupling for reverse rate constant.

Calculating reverse rate constant.

The reverse rate constant k(E) is multiplied by reaction path degeneracy equals to 1

 Canonical reverse rate constant, k(T)

  T(K)   Landau-Zener   Weak Coupling

  296.0  8.76E+01    3.50E+02
  297.0  9.50E+01    3.76E+02

Total CPU time =  4.40
NAST terminated now.
```

Calculations of the transition probabilities and rate constants between individual M_S components of the singlet and triplet states were carried out using the spin-orbit matrix elements (z = -69.0 – 63.8i cm^{-1} and b = 21.3 cm^{-1}), as defined in equation 2.22 obtained from SOC MCQDPT2 calculation. The M_S-specific rate constants $k_{M_S\,,\,M_{S'}}$ for the transitions between the $M_S = 0$ component of singlet state and three $M_{S'} = \pm 1$ and $M_{S'} = 0$ components of the triplet state, calculated using the LZ transition probability are plotted in Figure 5.7. The stronger couplings between the $M_S = 0$ component of the singlet state and the $M_{S'} = \pm 1$ components of the triplet result in the faster population transfer, as evident from the $k_{0,\pm 1}$ rate constant being larger than $k_{0,0}$.

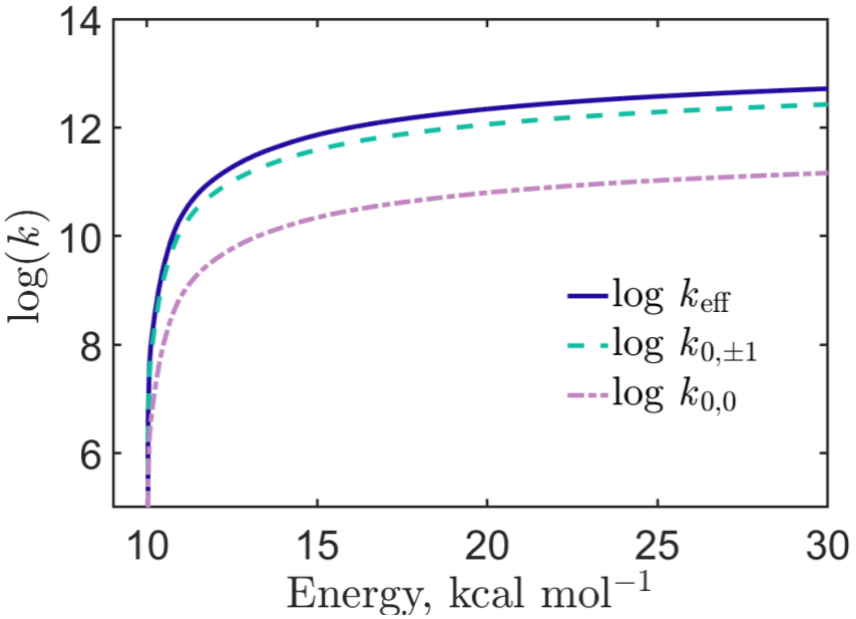

Figure 5.7. The microcanonical rate constants $k_{0,0}$ and $k_{0,+1} = k_{0,-1}$ for transitions between the M_S components of the singlet and triplet states calculated using the LZ probabilities.

References

(23) McGarvey, J.; Wilson, J. Photochemical Pertrurbation and Chemical Relaxation of the Planar - Tetrahedral Equilibrium in a Di(Tertiary Poshpine) Complex of Nickel(II). *J. Am. Chem. Soc.* **1975**, 2531–2532.

5.5. Example 5. $T_1 \rightarrow S_0$ relaxation in thiophosgene in tunneling regime

In this example we test the rate constant calculation using the Zhu-Nakamura transition probability formulas based on the $T_1 \rightarrow S_0$ relaxation in thiophosgene (Figure 5.8). Fujiwara et al.[33,34] measured lifetimes of the lowest vibrational states of the T_1 state for $CSCl_2$ molecule using the optical-optical double resonance technique. Energies of these vibrational states are all under the transition barrier. Therefore, the $T_1 \rightarrow S_0$ relaxation observed in experiment, is proceeding exclusively in the quantum tunneling regime. Experimental rate constants of transitions from these vibrational states of T1, obtained as inverse of the corresponding lifetimes, turned out to be in disagreement of around three orders of magnitude with estimates in multiple theoretical investigations[35,36]. Recently, we used the NAST package to calculate tunneling rates of the $T_1 \rightarrow S_0$ relaxation in thiophosgene using the WC and ZN transition probabilities.[2]

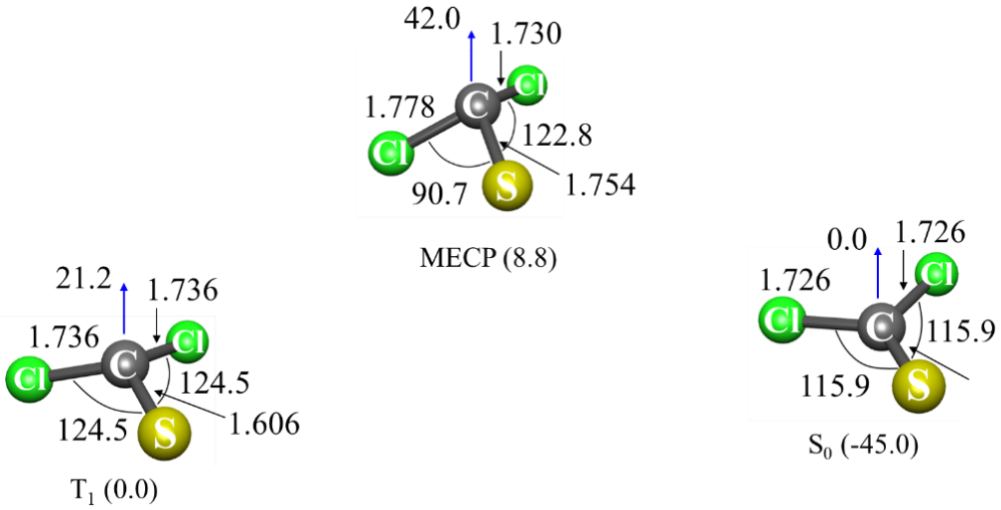

Figure 5.8. CASPT2/def2-TZVP optimized geometries for T_1, S_0 and MECP in thiophosgene. Blue arrows indicate the angle between Cl-S-Cl plane and C atom.

Input file

```
&keys zn =.true. zpe = 2 printmore = .true.  extern = .true. &end

&inputdata
chir = 2
freX = 244, 311, 490, 795, 919
freR = 174, 247, 489, 848, 926
inertX = 488.923, 569.396, 1048.550
inertR = 506.042, 555.108, 1052.703
enX = -1355.021
enR = -1355.036
maxn = 1000                    ! All calculations are in tunneling regime.
&end

&external
extR = 0, 298, 303, 563, 601, 795, 915      ! Double well levels.
&end

&probability
redmass = 14.6302
soc = 189
grad = 0.085073
gradmean = 0.077815
&end

&polynomials
hs4 = 0.025062
hs3 = -0.025452
hs2 = 0.0283647
hs1 = -0.001514
hs0 = 0.000016
```

```
ls4 = -4.847727
ls3 = 14.218237
ls2 = -15.528009
ls1 = 7.61989931
ls0 = -1.43837683
limitL = 0
limitR = 0.9
upper = .true.
&end
```

Main parts of the output file

```
 ******************************************************
 ~~~~~~~ NAST: Nonadiabatic Statistical Theory ~~~~~~~~
          ~~~~~ v. 2021.1 ~~~~~
 ******************************************************
------------------------------------------------------------
   NAST control parameters and related data
 zpe = 2    sp = F    zn = T    solution = F
 tst = F    printmore = T    rev = F    extern = T
------------------------------------------------------------
zpe = 2: ZPE correction scheme II (accounts for turning points below ZPE).
Electronic barrier from reactant to MECP is  3185 cm-1
ZPE of reactants =  0.00 cm-1
ZPE of MECP =  0.00 cm-1
ZPE-corrected MECP energy bin = 3186 cm-1
------------------------------------------------------------
       Start NAST calculation
------------------------------------------------------------
1. Calculating densities of states
.....vibrational.
.....rotational.
.....rovibrational.

 2. Calculating microcanonical probabilities
.....Landau-Zener

Warning! Rate calculations using transition probabilities that account
for quantum tunneling should be run with caution.
Make sure that in a reaction studied, reactant lies higher in energy than product.
Otherwise, there will be a region of unphysical tunneling, which should be excluded.
If this is the case, run a reverse (rev = .true.) calculation. This will allow NAST to prevent
unphysical tunneling. Details on reverse rate calculations can be found in the NAST package manual.

.....Weak Coupling
.....Zhu-Nakamura
     Sloped intersection of PESs
     Origin is High-Spin state at limitL
     Origin is at  0.00 bohr
```

```
 3. Calculating microcanonical NAST rate constant
  (The forward rate constant k(E) is multiplied by reaction path degeneracy equal to 2 ).

            Canonical rate constant, k(T).

  T(K)  Landau-Zener  Weak Coupling  Zhu Nakamura

  296.0  0.00E+00    2.04E+08    9.00E+05
  297.0  0.00E+00    2.05E+08    9.06E+05

Landau-Zener (LZ) and Weak Coupling (WC) double passage velocity-averaged
            probabilities of transition, p(T)
     Calculated using Maxwell-Boltzmann (MB) and Kuki (K)
            energy distributions

  T(K)  LZ MB   LZ K   WC MB   WC K

  296.0  0.6823  0.4628  0.0142  0.0001
  297.0  0.6819  0.4623  0.0142  0.0001

Total CPU time =  6.01
NAST terminated now.
```

In this example, we compare microcanonical calculated and experimental rate constants, and thus do not devote particular attention to canonical (temperature) rate constants (Table 5.2).

Table 5.3. Microcanonical rate constants for $T_1 \rightarrow S_0$ relaxation from lowest vibrational levels of T_1.

Vibrational mode, cm^{-1}	k_{WC}, s^{-1}	k_{ZN}, s^{-1}	Experiment[34], s^{-1}
0	7.87×10^{5}	6.07×10^{1}	4.40×10^{7}
247	1.66×10^{8}	7.14×10^{4}	5.90×10^{7}
494	4.31×10^{8}	6.29×10^{5}	8.00×10^{7}

We see that rate constants calculated using the WC transition probability formula are in reasonable agreement with experimental values. However, such agreement must be accidental, since the WC formula, derived from assumption of the linear crossing potentials in the vicinity of intersection of two states, underestimates the contribution of quantum tunneling. In contrast, the ZN approach accounts more accurately for tunneling by letting an arbitrary shape of the crossing potentials.[2] Thus, the discrepancy between WC and ZN results is the largest at small energies where the barrier width is maximum. The two order of magnitude discrepancy between experimental results and ZN-predicted rate constants reflects the complexity of the $T_1 \rightarrow S_0$ relaxation in thiophosgene and suggests that a role of multidimensional tunneling should considered[2].

References

(2) Lykhin, A. O.; Varganov, S. A. Intersystem Crossing in Tunneling Regime: T1 → S0 Relaxation in Thiophosgene. *Phys. Chem. Chem. Phys.* **2020**, *22* (10), 5500–5508. https://doi.org/10.1039/c9cp06956a.
(33) Fujiwara, T.; Moule, D. C.; Lim, E. C. Optical-Optical Double Resonance Probe of the Dark State of Thiophosgene in Supersonic Free Jet. *Chem. Phys. Lett.* **2004**, *389* (1–3), 165–170. https://doi.org/10.1016/j.cplett.2004.03.093.
(34) Fujiwara, T.; Lim, E. C. Temporal Characteristics of the S1 and T1 Thiophosgene Cl2 CS in the Gas Phase: Comparison of the T1 Decay with Theoretical Predictions. *J. Chem. Phys.* **2008**, *129* (4), 1–5. https://doi.org/10.1063/1.2963037.
(35) Moule, D. C.; Burling, I. R.; Liu, H.; Lim, E. C. The Cavity Ringdown Spectrum of the Visible Electronic System of Thiophosgene: An Estimation of the Lifetime of the T1(ã 3A2) Triplet State. *J. Chem. Phys.* **1999**, *111* (11), 5027–5037. https://doi.org/10.1063/1.479760.
(36) Rashev, S.; Moule, D. C.; Djambova, S. T. On the T1 → S0 Intersystem Crossing Rate Constant in Thiophosgene. *Chem. Phys. Lett.* **2007**, *441* (1–3), 43–47. https://doi.org/10.1016/j.cplett.2007.04.093.

5.6. Example 6. $T_1 \rightarrow S_0$ relaxation in cyclopropene

This example demonstrates calculation of the rate constant using the ZN transition probability. Miller and Klippenstein published a detailed kinetics study of different reactions of C_3H_4, including those proceeding on multiple PESs with different spin multiplicities.[37] Here we consider the $T_1 \rightarrow S_0$ relaxation in cyclopropane (Figure 5.9). The equilibrium geometries and Hessians of S_0, T_1 and MECP were obtained at the B3LYP/cc-pVTZ level of theory. The SOC constant of 4.0 cm^{-1} was calculated with the MCQDPT2 method based on the CASSCF(2,2) wave function averaged over the S_0 and T_1 states, using the same basis set. All calculations were performed in GAMESS.

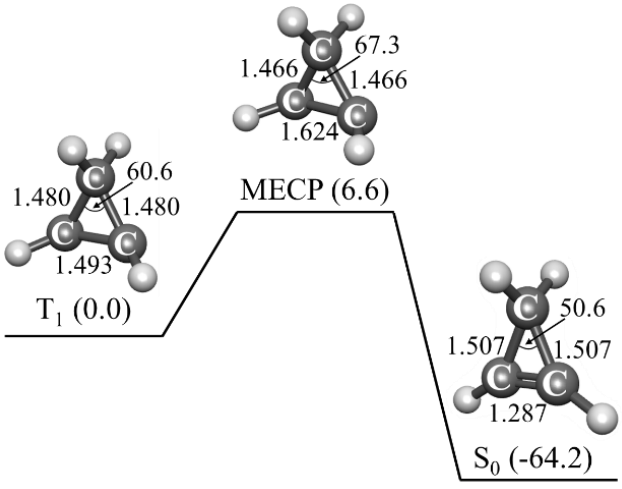

Figure 5.9 The $T_1 \rightarrow S_0$ relaxation pathway in cyclopropene. The relative energies of the T_1 minimum, the S_0 minimum and MECP are in kcal mol^{-1}. The bond lengths and angles calculated at the B3LYP/cc-pVTZ level of theory are in Å and degrees.

To perform the rate calculations with the ZN transition probability, the $T_1 \rightarrow MECP \rightarrow S_0$ reaction pathway was fitted with the *ircifit* tool using the geometries and energies generated by two IRC calculations starting from MECP and following to the T_1 and S_0 minima. The MECP$\rightarrow T_1$ pathway was fitted with the quartic polynomial, while MECP$\rightarrow S_0$ is linear between the T_1 minimum and MECP (Figure 5.10). The NAST input and output files are given below.

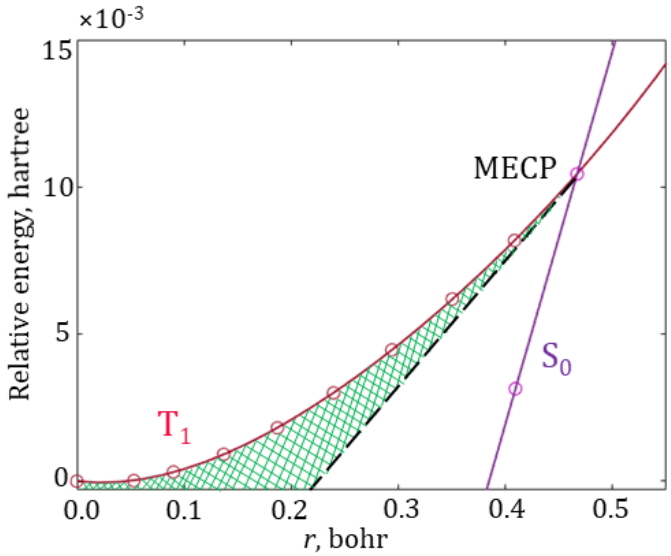

Figure 5.10 The fitted $T_1 \rightarrow MECP \rightarrow S_0$ reaction pathway. The circles mark the energies of the IRC geometries projected on the reaction coordinate *r*. Green area shows an increase in the tunneling barrier width compared to the linear model (dashed black line). The coefficients of the fitting polynomials ($f(x) = 0.092\,x^4 - 0.121\,x^3 + 0.093\,x^2 - 0.004\,x - 1.86 \times 10^{-6}$ and $g(x) = 0.127\,x - 0.048$) are included in the NAST input file.

Input file

```
$keys zpe = 1 printmore = .true. zn = .true. &end

&inputdata
freX = 399, 622, 797, 860, 947, 1002, 1132, 1182, 1290, 1344, 2868, 3096, 3110, 3117
inertX = 70.65814, 82.17973, 131.86505
freR=468, 715, 746, 865, 923, 935, 1031, 1070, 1098, 1259, 1399, 3000, 3087, 3140, 3156
inertR = 72.16025, 75.97359, 129.26232
enX=0.010435
enR=0
maxn=17000
T1=900
Tstep=100
T2=1000
```

```
&end

&probability
redmass=2.59106
soc=4
grad=0.144858
gradmean=0.123021
&end

&polynomials
hs4 = 0.09147
hs3 = -0.1207
hs2 = 0.09307
hs1 = -0.004072
hs0 = -0.000001816
ls4 = 0.00000
ls3 = 0.00000
ls2 = 0.00000
ls1 = 0.12690
ls0 = -0.0488
limitL = 0.0
limitR = 1.10
&end
```

Main parts of the output file

```
 ******************************************************
 ~~~~~~~ NAST: Nonadiabatic Statistical Theory ~~~~~~~~
          ~~~~~ v. 2021.1 ~~~~~
 ******************************************************
 ------------------------------------------------------
   NAST control parameters and related data
  zpe = 1   sp = F   zn = T   solution = F
  tst = F   printmore = T   rev = F   extern = F
 ------------------------------------------------------
zpe = 1: ZPE correction scheme I (eliminates turning points below ZPE).
Electronic barrier from reactant to MECP is 2290 cm-1
ZPE of reactants = 11444 cm-1
ZPE of MECP = 10881 cm-1
ZPE-corrected MECP energy bin = 1728 cm-1
 ------------------------------------------------------
        Start NAST calculation
 ------------------------------------------------------
  1. Calculating densities of states
.....vibrational.
.....rotational.
.....rovibrational.
  2. Calculating microcanonical probabilities
    LZ formula is valid at energies much greater than 4031 cm-1.
.....Landau-Zener
```

```
Warning! Rate calculations using transition probabilities that account
for quantum tunneling should be run with caution.
Make sure that in a reaction studied, reactant lies higher in energy than product.
Otherwise, there will be a region of unphysical tunneling, which should be excluded.
If this is the case, run a reverse (rev = .true.) calculation. This will allow NAST to prevent
unphysical tunneling. Details on reverse rate calculations can be found in the NAST package manual.

.....Weak Coupling
.....Zhu-Nakamura

     Sloped intersection of PESs
     Origin is High-Spin state at limitL
     Origin is at  0.00 bohr

  3. Calculating microcanonical NAST rate constant
   (The forward rate constant k(E) is multiplied by reaction path degeneracy equal to 1).

       Canonical rate constant, k(T).

   T(K)  Landau-Zener  Weak Coupling  Zhu Nakamura

   900.0  5.57E+07    1.05E+08    2.09E+07
  1000.0  7.72E+07    1.24E+08    3.07E+07

Landau-Zener (LZ) and Weak Coupling (WC) double passage velocity-averaged
             probabilities of transition, p(T)
      Calculated using Maxwell-Boltzmann (MB) and Kuki (K)
             energy distributions

   T(K)   LZ MB   LZ K    WC MB   WC K

  900.0  0.0002  0.0000  0.0000  0.0000
 1000.0  0.0002  0.0000  0.0000  0.0000

Total CPU time = 106.05
NAST terminated now.
```

The NAST calculated rate constants (Table 5.4) show that the use of the WC transition probability formula overestimates the rate constant when compared to the LZ and ZN formulas. This is due to overestimated contribution to rate constants from quantum tunneling in the WC linear-crossing model. As predicted by more sophisticated ZN theory, the real barrier width is significantly larger due to the nonlinear form of the T_1 state potential (green area in Figure 5.10). As a consequence, the reaction rate constant predicted using the ZN formulas is an order of magnitude smaller than the WC results. The match between the LZ- and ZN-rate constants can be explained by two effects. First, the large barrier width practically neglects the tunneling contribution to the reaction rate. Second is an inaccuracy of fitting potentials at higher energies above MECP. It is important to remember that the IRC points, used to fit the potentials, correspond to energies at or lower than MECP. Therefore, fitting procedure has no information about higher-energy points along the potentials and, therefore, the crossing potentials are merely extrapolations when above MECP.

Table 5.4. Canonical rate constants (s^{-1}) for the $T_1 \rightarrow S_0$ relaxation of cyclopropene at T = 900 – 1000 K.

Temperature	Landau-Zener	Weak Coupling	Zhu-Nakamura
900	5.57×10^{7}	1.05×10^{8}	2.09×10^{7}
1000	7.72×10^{7}	1.24×10^{8}	3.07×10^{7}

The Table 5.5 demonstrates good agreement between the canonical $T_1 \rightarrow S_0$ relaxation rate constants calculated in the NAST and MESMER 6.0 packages[29] using the LZ transition probabilities.

Table 5.5 The $T_1 \rightarrow S_0$ relaxation rate constant (s^{-1}) for different temperatures. Relative difference between the NAST and MESMER values is defined as $(k_{NAST}-k_{MESMER})/k_{MESMER}$.

T, K	MESMER	NAST	Relative difference
100	2.37×10^{-16}	1.52×10^{-16}	-0.36
200	7.88×10^{-4}	6.71×10^{-4}	-0.15
300	1.29×10^{1}	1.19×10^{1}	-0.08
400	1.68×10^{3}	1.62×10^{3}	-0.03
500	3.09×10^{4}	3.16×10^{4}	0.02
600	2.13×10^{5}	2.33×10^{5}	0.09
700	8.43×10^{5}	9.81×10^{5}	0.16
800	2.35×10^{6}	2.91×10^{6}	0.24
900	5.18×10^{6}	6.81×10^{6}	0.32
1000	9.71×10^{6}	1.35×10^{7}	0.39
1100	1.62×10^{7}	2.36×10^{7}	0.46
1200	2.47×10^{7}	3.75×10^{7}	0.52
1300	3.52×10^{7}	5.55×10^{7}	0.58
1400	4.76×10^{7}	7.74×10^{7}	0.63
1500	6.17×10^{7}	1.03×10^{8}	0.67
1600	7.73×10^{7}	1.31×10^{8}	0.69
1700	9.42×10^{7}	1.63×10^{8}	0.73
1800	1.12×10^{8}	1.96×10^{8}	0.75
1900	1.31×10^{8}	2.31×10^{8}	0.77
2000	1.50×10^{8}	2.67×10^{8}	0.78

References

(37) Miller, J. A.; Klippenstein, S. J. From the Multiple-Well Master Equation to Phenomenological Rate Coefficients: Reactions on a C3H4 Potential Energy Surface. *J. Phys. Chem. A* **2003**, *107* (12), 2680–2692. https://doi.org/10.1063/5.0046438.

6. Tools

6.1. Effective Hessian code

The source code of the Effective Hessian is available for Linux as a part of NAST package.

6.1.1. Introduction to Effective Hessian

The rate constant calculations require the knowledge of the rovibrational states at critical points of a reaction. The vibrational states at MECP are described by an effective Hessian matrix, composed of two spin state-specific Hessian matrices. As the traditional packages of electronic structure calculations do not support effective Hessian calculation, the *effhess* tool was designed.

The program requires gradients and Hessian matrices of two spin states at the MECP. Currently, the program supports reading input data from GAMESS and Molpro electronic

structure programs. The program generates an output file .out containing the $\boldsymbol{\nu}_X$ and $\boldsymbol{I}_X$ vibrational frequencies and principal moments of inertia at MECP, correspondingly, as well as the reduced mass $\mu_\perp$, the $|\Delta\mathbf{g}|$ norm of the gradient parallel to the reaction coordinate, and $\bar{\mathbf{g}} = (|\mathbf{g}_1||\mathbf{g}_2|)^{1/2}$ mean gradient.

6.1.2. Working equations

To perform vibrational analysis at the MECP, one needs to build the effective Hessian matrix:

$$\mathbf{H}_{\text{eff}} = \frac{|\mathbf{g}_1|\mathbf{H}_2 \pm |\mathbf{g}_2|\mathbf{H}_1}{|\mathbf{g}_1| \pm |\mathbf{g}_2|}, \tag{6.1}$$

where $\mathbf{g}$ and $\mathbf{H}$ are state-specific gradients and Hessian matrices obtained from electronic structure calculations. We perform projection of the mass-weighted effective Hessian (MWEH) to confirm seven zero frequencies associated with the translational, rotational and reaction coordinate (RC) degrees of freedom:

$$\mathbf{H}_{\text{proj}} = (\mathbf{I} - \mathbf{P})\mathbf{H}_{\text{eff}}^{\text{mw}}(\mathbf{I} - \mathbf{P}), \tag{6.2}$$

where $\mathbf{I}$, $\mathbf{H}_{\text{eff}}^{\text{mw}}$ and $\mathbf{P} = \mathbf{P}_{\text{tr}} + \mathbf{P}_{\text{rot}} + \mathbf{P}_{\text{rc}}$ are the identity, MWEH and projection matrices, correspondingly. To avoid linear dependence between projected eigenvectors, we separately project the MWEH onto $\mathbf{P}_{\text{rc}}$ to define the reaction coordinate eigenvector to calculate reduced mass along RC at MECP:

$$\mathbf{H}_{\text{proj}}^{\text{RC}} = \mathbf{P}_{\text{rc}}\mathbf{H}_{\text{eff}}^{\text{mw}}\mathbf{P}_{\text{rc}}. \tag{6.3}$$

The $\mathbf{H}_{\text{proj}}^{\text{RC}}$ matrix is then diagonalized to confirm a single non-zero eigenvalue, associated with RC. All the other degrees of freedom were projected out. The corresponding eigenvector $\mathbf{k}$ is then mass-weighted ($\mathbf{k}^{\text{mv}}$) by dividing its each component by the square root of mass of the corresponding atom. The reduced mass along RC is then calculated as an inverse scalar product of $\mathbf{k}^{\text{mv}}$ with itself:

$$\mu_\perp = (\mathbf{k}^{\text{T,mv}}\,\mathbf{k}^{\text{mv}})^{-1}. \tag{6.4}$$

Moreover, the *effhess* code allows user to visualize the nuclear motion along RC at the MECP or visualize displacements along imaginary normal mode(s) if any found upon diagonalization of the effective Hessian. There is always a chance that the MECP search converged only in the vicinity of real MECP, and the current geometry is therefore not a

stationary point on intersection of two PESs. To visualize nuclear motion, we generate cartesian displacements from MECP equilibrium geometry along the selected degree of freedom (RC or imaginary frequency mode) using the corresponding eigenvector Q. in case of RC, we diagonalize $\mathbf{H}_{\mathrm{proj}}^{\mathrm{RC}}$ to get the vector $\mathbf{k}$. In case of imaginary frequency(ies), we use eigenvector(s) Q from diagonalized $\mathbf{H}_{\mathrm{proj}}$ that correspond(s) to imaginary frequency mode(s). The general formula for generating displacements is:

$$\mathbf{x} = \mathbf{x}_0 + \mathrm{D}\mathbf{Q}, \tag{6.5}$$

where $\mathbf{x}_0$ describes MECP nuclear geometry, D is scaled displacement, $\mathbf{Q}$ is selected normal mode and $\mathbf{x}$ is generated Cartesian geometry along $\mathbf{Q}$.

6.1.3. Installation

The installation process of *effhess* is identical to the one described for the NAST main code in 1. Installation Guide. Up to now, the compilation of the source code has been tested for

- GNU Fortran (GCC) 8.2.0 compiler
- ifort (IFORT) 13.0.0 20120731 compiler
- Intel® MKL 2018.2.199 – 2018.4.274
- Intel® MKL 2019.0.117 – 2019.5.281
- Intel® MKL 2020.0.166 Initial Release

Note: There are issues found when using Intel® MKL 2019.3.199 and above for GNU Fortran compiler. The test examples delivered artificial imaginary frequencies when diagonalizing the EH. Therefore, our recommendation would be to use either Intel compiler with all the libraries listed above or use GNU compiler with MKL no higher than 2019.2.187.

6.1.4. Running Effective Hessian (effhess.x)

To run the executable, you need the math library to be run-time accessible: modify your PATH and LD_LIBRARY_PATH environmental variables to include

```
export PATH = $PATH:/…/compilers_and_libraries_20XX.X.XXX/linux/bin
export LD_LIBRARY_PATH = $LD_LIBRARY_PATH: /…/intel/…/linux/mkl/lib/intel64
```

For your convenience, you might want to give an alias to executable to access that across all directories. For example, modify your .bash_profile to include the path to executable

```
alias effhess = '/path/to/effhess.x'
```

and then source .bash_profile. Now invoke calculations with *effhess Inputfile.*

6.1.5. Input structure

Let's imagine you are interested in an R → MECP → P spin-forbidden reaction, where R, MECP and P are reaction reactant, MECP and product, respectively. Note that we define reactant as a minimum of the excited state. Therefore, the R → MECP pathway is a relaxation process. Say you are modeling the forward R → MECP reaction and you have found the MECP between two electronic states with different spin multiplicities, say singlet and triplet states. Your program of choice was GAMESS electronic structure program. You now use this MECP geometry to run two hessian calculations at each spin multiplicity to obtain $\mathbf{g}$ and $\mathbf{H}$ state-specific gradients and Hessian matrices. Names of your GAMESS Hessian input files are *mecp_hessian_singlet.inp* and *mecp_hessian_triplet.inp*, correspondingly. The respective *.dat* files contain gradients and Hessian data. Then, the *effhess* input file will contain the following lines:

Example of Effective Hessian input file

```
&programs GAMESS = .true. &end

&games_input_files
low_spin_dat = 'mecp_hessian_singlet.dat'
high_spin_dat = 'mecp_hessian_triplet.dat'
input_geometry = 'mecp_hessian_singlet.inp'
&end
```

End of example

6.1.6. Navigation through output files

There are three (plus one optional) output files generated by the *effhess* code. They contain molecular properties at MECP for the NAST input data. **Note:** the only property remained to be provided to the NAST input file is the SOC constant, which comes directly from electronic structure calculations.

.out — The **.out** file is the main output file of the effective Hessian code. It contains the bullet points from vibrational analysis at MECP. These include the intersection type of two PESs as well as various gradient data like geometric mean of two gradients ($\bar{\mathbf{g}}$, hartree/bohr), norm of the gradient parallel to the reaction coordinate ($|\Delta\mathbf{g}|$,

hartree/bohr), the reduced mass $\mu_\perp$ (amu) at MECP, vibrational frequencies, ZPE and principal moments of inertia. These data forms MECP part of the NAST input. In addition, calculated data is put separately into the **.nast** output file, which can be used as the template for the NAST input file (see below). What is left is the SOC value at MECP, which should be provided by user in the NAST input file.

.imag There is always a chance that found MECP geometry is not accurate enough and is therefore not a stationary point on intersection of two PESs. If it is the case, then the vibrational analysis at this geometry will show one or multiple imaginary frequency modes. It means that the MECP re-search is needed. The **.imag** file offers aid in this respect. Note: The file will be generated only if there are imaginary frequencies found. Let's say there are two imaginary frequency modes. Then, for each of them, a list of Cartesian coordinates will be generated by sampling displacements along an imaginary frequency mode. The default is to generate twenty displacements. Therefore, for two imaginary modes, there will be a total of forty cartesian geometries that correspond to displacements along either of the modes. User is free to choose any of those geometries as a starting guess for the MECP re-search.

.rc Resembles the **.imag** file; the **.rc** file contains Cartesian geometries generated along displacements along the reaction coordinate mode. Can be used to visualize the reaction coordinate at the MECP.

.nast The NAST template input file that contains the MECP-part data: $\bar{\mathbf{g}}$, $|\Delta\mathbf{g}|$, $\mu_\perp$, $\boldsymbol{\nu}_\mathrm{X}$ and $\boldsymbol{I}_\mathrm{X}$.

6.1.7. Example 1. Effective Hessian for methoxy cation, CH_3O^+

Let us construct an effective Hessian for the example of spin-forbidden dehydrogenation of the triplet methoxy cation, $^3CH_3O^+$ (5.1. Example 1). An input to the effective Hessian code are the state-specific gradients and hessian matrices at MECP geometry, and the MECP geometry itself. Let us run two effective Hessian calculations using input data from two different electronic structure methods and compare the results. Since the state-specific Hessians depend only weakly on the level of theory, then the method-specific input data should be close enough to each other to expect two effective Hessian matrices to be the same within numerical accuracy. Of course, this is true only if two levels of theory predict close MECP structures. Our choice is GAMESS B3LYP and Molpro CCSD(T) methods. The cc-pVTZ basis set is used. We first run respective electronic structure calculations to locate the minimum of reactants and the MECP structure, then use the corresponding data as input for two independent Effective Hessian runs, and finally compare the results. Hence, the structure of this example looks as following:

1. Effective Hessian from GAMESS B3LYP gradients and state-specific Hessians;
2. Effective Hessian from Molpro CCSD(T) gradients and state-specific Hessians;
3. The comparison of results;
4. **.nast** and **.rc** output: NAST input template and visualization of the reaction coordinate.

1. Effective Hessian from GAMESS B3LYP gradients and state-specific hessians.

Let us create an input file, *meth_cation_eff_hess_GAMESS.com*, where we specify names of the GAMESS *.dat* and *.inp* files to be read by *effhess*. The *.dat* files for each spin contain respective gradients and Hessians. The MECP search was performed as implemented in GAMESS. The *.inp* file is used to read the MECP nuclear geometry. Given an alias - **alias effhess = '/path/to/effhess.x'** – has been added to the **.bash_profile**, execution of the code becomes:

effhess meth_cation_eff_hess_GAMESS.com

meth_cation_eff_hess_GAMESS.com:

```
&programs GAMESS = .true. &end

&games_input_files
low_spin_dat = 'meth_cation_mecp_geometry_s.dat'
high_spin_dat = 'meth_cation_mecp_geometry_t.dat'
input_geometry = 'meth_cation_mecp_geometry_s.inp'
&end
```

meth_cation_eff_hess_GAMESS.out (some headers skipped):

```
                ******************************************************************
                  ~~~~~~~ Effective Hessian: part of NAST package ~~~~~~~~
                                    ~~~~~ v. 2021.1 ~~~~~
                ******************************************************************

Opening the methoxy_cation_eff_hess.inp input file

Effective Hessian data

Gradmean =  8.190326591E-02
Norm of parallel gradient =  1.657563917E-01
Norm of low-spin gradient =  7.020334815E-02
Norm of high-spin gradient =  9.555306327E-02
Lambda =  0.423533E+00
Gradients dot product = -6.708141697E-03 indicates PEAKED intersection

Principal moments of inertia (amu*bohr**2)

                          12.084982390  56.731153496  57.962092062

Frequency (cm-1)      Reduced mass (amu)
          0.00           3.6577635
          0.00           1.4484445
          0.00           1.7494525
          0.00           2.4888227
          0.00           3.8202261
          0.00           1.8795309
          0.00           6.3846805
     670.56              1.0652821
     1063.90             1.2606661
     1093.35             1.1924504
     1301.17             2.0051169
     1429.34             1.6200189
     2071.39             1.0750162
     2855.30             1.0358111
     2966.86             1.1137742

Reduced mass along the reaction coordinate (amu):  1.3188641
zpe in kcal mol-1:  19.23042629
```

```
Total CPU time =  0.050
```

2. Effective Hessian from Molpro CCSD(T) gradients and state-specific hessians.

An input file, *meth_cation_eff_hess_Molpro.com*, contains names to the Molpro output files, *.out*. Note that in case of Molpro, state-specific gradients and Hessians are stored in separate files. Therefore, in case of using Molpro, more input files should be provided compared to GAMESS. Since the MECP search is not implemented in the Molpro version used in this work, we interfaced the external Harvey script. Gradients are read from final state-specific single-point calculation output files at the MECP geometry. The Hessians are read from respective output files at the MECP geometry. The MECP coordinates are read from one of gradient output files. Therefore, there is a total of four input file names: spin_1_grad.out, spin_1_hess.out, spin_2_grad.out, spin_2_hess.out to be provided in *meth_cation_eff_hess_Molpro.com.* Below are contents of the *meth_cation_eff_hess_Molpro.com* and *meth_cation_eff_hess_Molpro.out* files:

meth_cation_eff_hess_Molpro.com:

```
&programs Molpro = .true. &end

&molpro_input_files
low_spin_grad = 'low_grad_mecp_geometry.out'
high_spin_grad = 'high_grad_mecp_geometry.out'
low_spin_hess = 'low_hess_mecp_geometry.out'
high_spin_hess = 'high_hess_mecp_geometry.out'
&end
```

meth_cation_eff_hess_Molpro.out (some headers skipped):

```
                    ********************************************************************
                      ~~~~~~~ Effective Hessian: part of NAST package ~~~~~~~~
                                      ~~~~~ v. 2021.1 ~~~~~
                    ********************************************************************


Opening the methoxy_cation_eff_hess.inp input file

Effective Hessian data

Gradmean =  7.785103926E-02
Norm of parallel gradient =  1.564105184E-01
Norm of low-spin gradient =  7.076154507E-02
Norm of high-spin gradient =  8.565081936E-02
Lambda =  0.452403E+00
Gradients dot product = -6.060495575E-03 indicates peaked intersection

Principal moments of inertia (amu*bohr**2)

        12.110459569  57.572646482  58.796000070
```

Frequency (cm-1)	Reduced mass (amu)
0.00	2.0622685
0.00	1.7794739
0.00	2.1473270
0.00	3.4686578
0.00	4.3118504
0.00	3.3434755
0.00	1.8844205
672.20	1.0803063
1068.04	1.2365189
1080.22	1.1981384
1284.86	2.4840173
1423.35	1.3717062
2125.98	1.0628045
2913.69	1.0358137
3033.15	1.1133256

Reduced mass along the reaction coordinate (amu): 1.3535208
zpe in kcal mol-1: 19.44427734
Total CPU time = 0.013

3. The comparison of results

In the Table 6.1. below we compare the NAST input data obtained from the above effective Hessian runs. For each input data, we calculate the absolute relative difference: $\Delta[X] = \left|X_{\text{GAMESS,DFT}} - X_{\text{Molpro,CCSD(T)}}\right| / \left|X_{\text{Molpro,CCSD(T)}}\right|$. For example, $\Delta[|\Delta\mathbf{g}|] = \left||\Delta\mathbf{g}|_{\text{GAMESS,DFT}} - |\Delta\mathbf{g}|_{\text{Molpro,CCSD(T)}}\right| / \left||\Delta\mathbf{g}|_{\text{Molpro,CCSD(T)}}\right|$ or $\Delta[\mu_\perp] = \left|\mu_{\perp\text{GAMESS,DFT}} - \mu_{\perp\text{Molpro,CCSD(T)}}\right| / \left|\mu_{\perp\text{Molpro,CCSD(T)}}\right|$ or $\Delta[\boldsymbol{I}_\text{X}] = \left|\boldsymbol{I}_{\text{X}_\text{GAMESS,DFT}} - \boldsymbol{I}_{\text{X}_\text{Molpro,CCSD(T)}}\right| / \left|\boldsymbol{I}_{\text{X}_\text{Molpro,CCSD(T)}}\right|$, where $\Delta[\boldsymbol{I}_\text{X}]$ is an average among *xx*-, *yy*-, and *zz*–principal components of the moments of inertia tensor.

Table 6.1. Comparison of the effective-Hessian-part of the NAST input data obtained from GAMESS and Molpro electronic structure programs.

$\Delta[\bar{\mathbf{g}}]$	$\Delta[\|\Delta\mathbf{g}\|]$	$\Delta[\mathbf{g}_1 \cdot \mathbf{g}_2]$	$\Delta[\mu_\perp]$	$\Delta[\boldsymbol{I}_\text{X}]$
0.052	0.059	0.107	0.025	0.010
$\{\Delta[\nu_{X,i}]\}_{i=1}^{8}$, where i runs through all vibrational modes at the MECP (3N-7) N = 5 for CH_3O^+				
0.002, 0.004, 0.012, 0.012, 0.004, 0.026, 0.020, 0.022				

There are few sources of discrepancy between respective data from two runs. One of them comes from the slightly different MECP structures predicted by two levels of theory. In Figure 6.1 we show structural parameters of B3LYP/cc-pVTZ and CCSD(T)/cc-pVTZ CH_3O^+ MECPs. We notice that the most prominent changes are in parameters related to the reaction coordinate and that involve the upper hydrogen in the plane of Figure: C-H bond length 1.242 vs. 1.224 Å, H-C-O angle ∠77.2° vs. ∠80.3° and C-O bond length 1.283 vs. 1.295 Å. Due to differences in geometries, we would expect slight differences in the geometry-dependent properties like frequencies and principal moments of inertia.

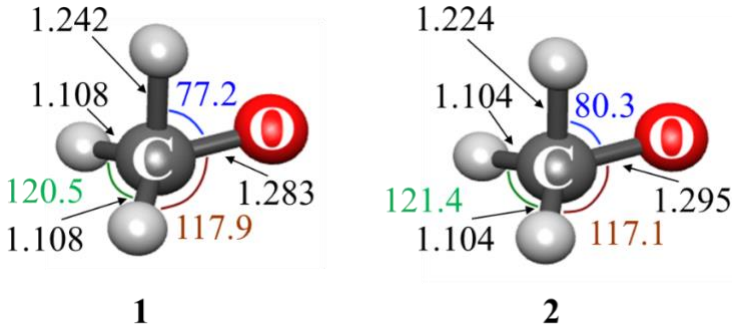

Figure 6.1. B3LYP/cc-pVTZ (**1**) and CCSD(T)/cc-pVTZ (**2**) CH_3O^+ MECP structures.

However, as seen from Table 6.1, the largest absolute relative differences are those for the gradient data: $\mathbf{g}_1 \cdot \mathbf{g}_2$, $\bar{\mathbf{g}}$ and $|\Delta\mathbf{g}|$. The reason for that, at least for GAMESS and Molpro versions used in this work, is different number of figures in printed gradients. GAMESS prints the gradient components in Fortran scientific notation format with eleven significant figures. For example:

```
$GRAD
E=    -114.6214870595  GMAX=   0.0413225  GRMS=   0.0181264
CARBON         6.   2.2253110167E-02  -4.1322469734E-02  -3.9992020539E-03
HYDROGEN       1.   1.0174276459E-02   4.2805715286E-03   2.5607227680E-02
…
$END
```

Therefore, the number of significant figures is fixed. On the other hand, Molpro prints the same data in Fortran F format for a string of ten-digit floating-point numbers:

```
Atom        dE/dx          dE/dy          dE/dz
  1     -0.029434150    0.053529845    0.003913258
  2     -0.009795518   -0.008059090   -0.029300563
 …
  5      0.029711615   -0.028674867    0.026025381
```

We see that in case of Molpro, different components of a gradient have different number of significant figures. Therefore, GAMESS and Molpro gradients have different accuracy. Therefore, there are two sources of discrepancy in results from these two effective Hessian runs: different levels of theory and different accuracy of electronic gradients. To eliminate the second source and directly compare results from two levels of theory, we cut the GAMESS gradients to the same number of significant digits by using the Molpro gradient format. We therefore cut GAMESS gradients inside the output files and then re-run effective Hessian using the GAMESS data once again.

As a result, we find only negligible impact on $\mathbf{g}_1 \cdot \mathbf{g}_2$, $\bar{\mathbf{g}}$ and $|\Delta\mathbf{g}|$ coming from cut gradients. The difference with respect to previous $\mathbf{g}_1 \cdot \mathbf{g}_2$, $\bar{\mathbf{g}}$ and $|\Delta\mathbf{g}|$ is only in eighth significant digit. Therefore, all the differences listed in Table 6.1. above come solely from difference in two electronic structure methods.

To get a final confirmation, let us run two NAST calculations with the same reactant data, same MECP barrier but different MECP-part data – $\bar{\mathbf{g}}$, $|\Delta\mathbf{g}|$, $\mu_\perp$, $\boldsymbol{I}_\mathrm{X}$ and $\boldsymbol{\nu}_\mathrm{X}$ – from the Molpro and GAMESS-cut-gradients effective Hessian runs. Below we compare ZPE-corrected MECP barriers and microcanonical and canonical rate constants at selected energies and temperatures:

GAMESS: ZPE-corrected MECP energy bin = 4751 cm^{-1} (13.6 kcal mol^{-1})
Molpro: ZPE-corrected MECP energy bin = 4826 cm^{-1} (13.8 kcal mol^{-1})

GAMESS: k_{WC}(E=1 cm^{-1}): 7.50E+03 k_{WC}(E=6000 cm^{-1}): 4.20E+09
Molpro: k_{WC}(E=1 cm^{-1}): 1.73E+04 k_{WC}(E=6000 cm^{-1}): 4.53E+09

GAMESS: k_{WC}(T=297 K): 2.97E+06 k_{WC}(T=298 K): 2.99E+06
Molpro: k_{WC}(E=297 K): 6.25E+06 k_{WC}(T=298 K): 6.28E+06

We see that the effect on the final rate constants is indeed small, which is after all expected as we effectively describe the same MECP structure with only small structural differences coming from two levels of theory.

4. .nast and .rc output: NAST input template and visualization of the reaction coordinate.

In this section we show additional effective Hessian output files. If successfully finished, the code generates the NAST input template *.nast* file that contains MECP part of the input data. For the example of the methoxy cation above, the *.nast* file looks the following:

methoxy_cation_eff_hess.nast:

```
! This is an NAST template input file automatically generated
! by the Effective Hessian code. The file contains the MECP part
! of NAST input. Check NAST manual to finish the input file.

&keys zpe=1 &end
```

```
&inputdata
freR =
freX = 671 1064 1093 1301 1429 2071 2855 2967
inertX= 12.08498  56.73115  57.96209
inertR =
enX =  enR =
redmass =  1.3188641 soc =
grad = 0.165756392 gradmean = 0.081903266
maxn = 10000
&end
```

Finally, in the *.rc* output file one can find Cartesian geometries that correspond to displacements along the reaction coordinate:

methoxy_cation_eff_hess.rc:

```
Geometry #  0
CARBON       6.0    -1.928645748     -0.006530451     -2.277655863
HYDROGEN     1.0     -1.164444021     -0.823984548      -1.702797871
HYDROGEN     1.0     -1.217219172      1.018216165       -2.125297851
HYDROGEN     1.0     -2.773842684       0.104946208      -1.354278063
OXYGEN       8.0    -2.547205994      0.021671629       -3.493235621
                                  ...
Geometry # 4
CARBON       6.0     -1.955420467      0.043203831       -2.272821423
HYDROGEN     1.0      -1.310216188      -0.885344623       -2.069726700
HYDROGEN     1.0      -1.177421821       0.924375917       -2.136209287
HYDROGEN     1.0      -2.721637543       0.018347865       -1.371313405
OXYGEN       8.0    -2.523730585     -0.000405434       -3.471981846
                                  ...
Geometry # 7
CARBON       6.0     -1.975501506       0.080504542       -2.269195592
HYDROGEN     1.0     -1.419545312      -0.931364679      -2.344923321
HYDROGEN     1.0     -1.147573808       0.853995731       -2.144392863
HYDROGEN     1.0     -2.682483687      -0.046600893      -1.384089912
OXYGEN       8.0    -2.506124029      -0.016963232      -3.456041515
                                  ...
```

One can visualize these displacements using a molecular editor program:

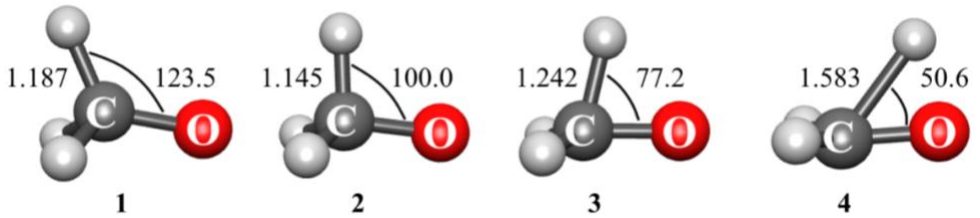

Figure 6.2. CH_3O^+ structures (1→4) generated by displacements along the reaction coordinate normal mode at MECP.

If upon diagonalization of effective Hessian, you find imaginary normal mode(s), the corresponding Cartesian geometries for each imaginary mode will be written in the *.imag* file. One can use one of these geometries to restart MECP search.

6.2. Intrinsic reaction coordinate fitting (*ircfit*)

The source code of *ircfit* is available for Linux as a part of the NAST package.

6.2.1. Introduction to *ircfit*

A perhaps central quantity in the kinetics theory of nonadiabatic processes is the probability of transition between states with different spin multiplicities. Typical two-state models, used to derive probability expressions, adopt a picture of two 1-D crossing electronic potentials. Many models assume constant slope of the potentials in the crossing region, that is, linear crossing. This assumption allows one to derive simple analytical expressions for transition probabilities, like Landau-Zener and Weak Coupling formulae (2.3 NAST working equations). The assumption of linear crossing means that explicit potentials, which represent the minimum energy path that connects reactant and product with the minimum on the crossing seam, are neglected.

Evidently, the linear crossing is generally not true. Therefore, the probability expressions derived from models that permit an arbitrary potentials' crossing shape would benefit in accuracy. For instance, the Zhu-Nakamura (ZN) transition probability formulas are one example of such models. The rate constant calculations that employ the ZN formulas require explicit crossing potentials as part of the input data. The *ircfit* code offers aid to obtain such potentials.

6.2.2. Methodology

The main idea behind intrinsic reaction coordinate (IRC) fit is to build one-dimensional electronic potentials for different spin multiplicities that 1) connect key stationary points of the reaction, namely reactant, MECP and product and 2) can be described by analytical continuous function, i.e., by polynomial, to provide access to any arbitrary point on the potential. To build the crossing potentials the *ircfit* tool does the following:

1) Read the IRC data from GAMESS suite of programs. User has to perform two IRC calculations in GAMESS to obtain the molecular geometries at the points between reactant and MECP, and between MECP and product. As input, IRC fit requires two *.log* GAMESS files. The IRC points are the collection of $\{\boldsymbol{Q}_i, E_i\}_{i=1}^{n+m}$, where $\boldsymbol{Q}_i$ and E_i are molecular structure and energy at point *i*, $\boldsymbol{Q}_1$ and E_1 are MECP geometry and energy, and n and m are the total numbers of IRC points for reactant and product, respectively. In general, n and m are different. The *ircfit* tool works independently with each of the GASMESS *.log* files. We plan to enable the *ircfit* tool to read IRC data from several other electronic structure packages in future releases.

2) Project the $\{\boldsymbol{Q}\}^{reac}$ and $\{\boldsymbol{Q}\}^{prod}$ nuclear geometries onto a chosen one-dimensional reaction coordinate r. Note that even though $\{\boldsymbol{Q}\}^{reac}$ and $\{\boldsymbol{Q}\}^{prod}$ geometries are found by

following different minimum energy paths, and therefore correspond to different multi-dimensional curvilinear coordinates, they have to be projected onto *single* one-dimensional reaction coordinate to represent crossing potentials.

We choose the minimum of reactants as the origin of the x-axis that represent single reaction coordinate r. Therefore, there is a single reference point for both sets of $\boldsymbol{Q}$s. Then, we convert a set of $\boldsymbol{Q}$s into *r* according to the arc length formula:

$$r_j = \left(\sum_{i=1}^{3N} (dQ_{j,i})^2 \right)^{1/2}, \qquad j = \overline{1, n+m} \tag{6.6}$$

where $dQ_{j,p}$ is the difference between Cartesian coordinates of the reference point and point j, where j runs over all IRC points. Obviously, the reference point will therefore be converted to zero as origin of the x-axis.

3) Fits the $\{r_i, E_i\}_{X \to R}$ and $\{r_i, E_i\}_{x \to P}$ data points to analytical continuous functions to obtain two one-dimensional crossing potentials, where *x* is one-dimensional reaction coordinate.

Note 1: We now choose the reference point for energy as the energy of the minimum of reactants. In the MECP → reactant IRC path, this will be the energy of the last point (first IRC point is MECP): E_n. Now, energies of all the points are referenced to E_n.

Note 2: for the MECP → product IRC path, we keep only those points, which energies are equal to or higher than zero, i.e., we keep only those product IRC points, which lie at or above the minimum of reactants. Therefore, the all the IRC points for product below the minimum of reactant are excluded.

The *ircfit* tool works with polynomials up to the fourth order. The choice of polynomial order is based on the numbers n and m, where m pertains *only* to the IRC points for a product *above* the minimum of reactants. If $n = 2$, so only two IRC points from MECP to minimum of reactant or product are provided, then the IRC path is fitted by a line, if $n = 3$ – by a parabola, if $n = 4$ – by a cubic polynomial, if $n \geq 5$ – by a quartic polynomial. Illustrative examples of polynomial fitting are shown in Figure 6.3.

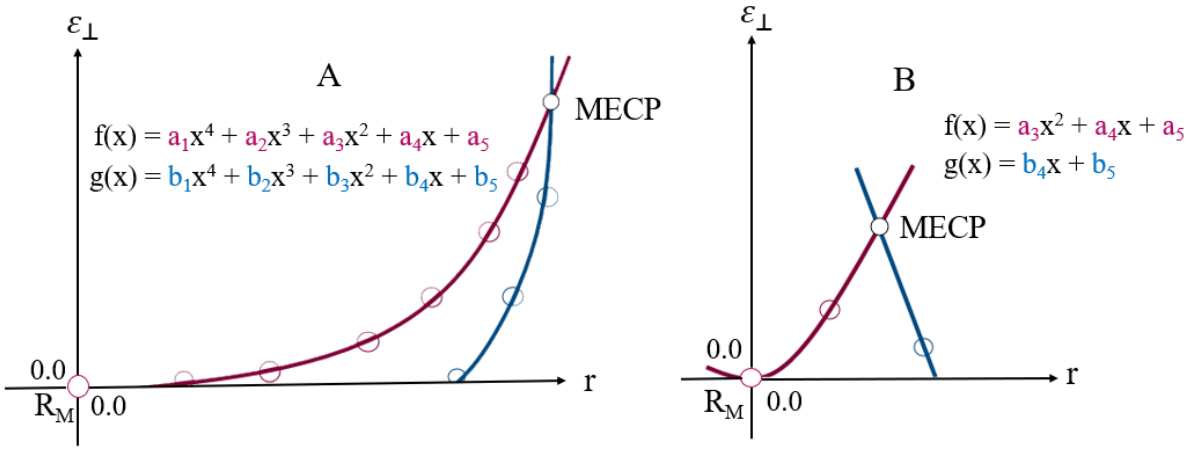

Figure 6.3 Illustrative examples of the fitted IRC paths along 1-D reaction coordinate r. R_M is the reactant minimum, $\varepsilon_\perp$ is energy component perpendicular to the crossing seam. A) Sloped-type intersection; reactant and product points are fitted to a quartic polynomial. B) Peaked-type intersection; reactant and product points are fitted to a parabola and a line, correspondingly.

The polynomial coefficients are found by solving the following system of linear equations:

$$f(\boldsymbol{c}, r) = \begin{cases} c_1 r^4 + c_2 r^3 + c_3 r^2 + c_4 r + c_5 \ \text{or} \\ c_2 r^3 + c_3 r^2 + c_4 r + c_5 \ \text{or} \\ c_3 r^2 + c_4 r + c_5 \ \text{or} \\ c_4 r + c_5 \end{cases}, \qquad (S49)$$

$$F = \sum_{i=1}^{k} \left(E_i - f(\boldsymbol{c}, r_i)\right)^2 \rightarrow \min(\boldsymbol{c}), \qquad (S50)$$

$$\frac{\partial F}{\partial \boldsymbol{c}} = 0,$$

where k is either n or m, and F is the non-linear least squares function.

6.2.3. Installation

The installation process is identical to the one described for the NAST main code. Up to now, the compilation of the source code has been tested with

- GNU Fortran (GCC) 8.2.0 compiler
- ifort (IFORT) 13.0.0 20120731 compiler
- Intel® MKL 2018.2.199 – 2018.4.274
- Intel® MKL 2019.0.117 – 2019.5.281

- Intel® MKL 2020.0.166 Initial Release

For more details, look at **1. Installation Guide**.

6.2.4. Running IRC fit (ircfit.x)

To run the irc.x executable, you need the math library to be run-time accessible: modify your PATH and LD_LIBRARY_PATH environmental variables to include

export PATH = $PATH:/…/compilers_and_libraries_20XX.X.XXX/linux/bin

export LD_LIBRARY_PATH = $LD_LIBRARY_PATH: /…/intel/…/linux/mkl/lib/intel64

For your convenience, you might want to give an alias to executable to access that across all directories. For example, modify your **.bash_profile** to include the path to executable

alias irc = '/path/to/irc.x'

and then source .bash_profile. Now invoke calculations with *irc inputfile*.

6.2.5. Input file syntax

Let's imagine you are interested in a R → MECP → P spin-forbidden reaction, where R, MECP and P are reactant, MECP and product, respectively. Note that we define reactant as a minimum of the excited state. Therefore, the R → MECP pathway is a relaxation process. Say you are modeling the forward R → MECP reaction and you have found the MECP between two electronic states with different spin multiplicities, say singlet (R) and triplet (P) states. Your program of choice was GAMESS electronic structure program. You now use this MECP geometry to run two irc calculations for each spin multiplicity to obtain minimum energy paths to minimum of R and P, correspondingly. Names of your GAMESS irc input files are *mecp_irc_reactant.inp* and *mecp_irc_product.inp*, correspondingly. The respective *.log* files contain irc geometries and respective electronic energies. Then, your irc fit input file will be the following:

Example of irc fit input file

```
&programs GAMESS = .true. &end

&games_input_files
g_irc_output_reac = 'mecp_irc_reactant.log'
g_irc_output_prod = 'mecp_irc_product.log'
&end
```

End of example

6.2.6. Navigation through output files

There are two output files generated by the *ircfit* code.

.out	The **.out** file is the main output file of the *ircfit* code. It contains the fitted polynomial coefficients and raw and fitted irc points to compare. The polynomial coefficients are used in the NAST input in the **&polynomials** group if ZN calculation is requested. In addition, coefficients are put separately into the **.nast** output file, which can be used as the template for the NAST input file.
.nast	The NAST template input file that contains the polynomial coefficients.

6.2.7. Example 1. Getting 1-D crossing potentials for $T_1 \rightarrow S_0$ relaxation in cyclopropene

In this example, we use our *ircfit* code to calculate coefficients of polynomials that approximate the 1-D crossing potentials of T_1 and S_0 states involved in relaxation in cyclopropene (5.6. Example 6. $T_1 \rightarrow S_0$ relaxation in cyclopropene). These coefficients are then used in the **&polynomials** group to model explicit spin-diabatic potentials. The irc calculation was as simple as:

```
[user@fe folder] ls
cyclopropene.inp irc_s.log irc_t.log
[user@fe folder] irc cyclopropene.inp
[user@fe folder] ls
cyclopropene.inp cyclopropene.out cyclopropene.nast irc_s.log irc_t.log
```

The contents of **.inp**, and sketches of **.out** and **.nast** files are shown below.

INPUT

```
&programs GAMESS = .true. &end

&games_input_files
g_irc_output_reac = 'irc_t.log'
g_irc_output_prod = 'irc_s.log'
&end
```

OUTPUT

```
                 ****************************************************************
                      ~~~~~~~ Intrinsic Reaction Coordinate fit ~~~~~~~~
                                    ~~~~~ v. 2021.1 ~~~~~
                 ****************************************************************

Opening the cyclopropene.inp input file
MECP-reactant minimum energy path has been fit to a quartic polynomial:

                          f(x) = a1*x^4 + a2*x^3 + a3*x^2 + a4*x + a5, where

                 a1 = 0.09146 a2 = -0.12069 a3 = 0.09307 a4 = -0.00407 a5 = -0.00000

The polynomial has been fit in the range of [0.000,0.467] bohr.

MECP-product minimum energy path has been fit to a line:

                                          g(x) = b1*x + b2, where

                                       b1 =   0.12693 b2 =   -0.04880

The polynomial has been fit in the range of [0.409,0.467] bohr.

MECP-reactant irc points, energies and energies fit from f(x)

n      x, Bohr     E, a.u.    E_fit, a.u.

1     0.46674     0.01044     0.01044
2     0.40844     0.00818     0.00818
3     0.35027     0.00619     0.00618
...
10     0.00000     0.00000    -0.00000

MECP-product irc points, energies and energies fit from g(x)

n      x, Bohr     E, a.u.    E_fit, a.u.

1     0.46674     0.01044     0.01044
2     0.40924     0.00314     0.00314

Total CPU time =  0.178
```

NAST

```
                 ****************************************************************
                      ~~~~~~~ Intrinsic Reaction Coordinate fit ~~~~~~~~
                                    ~~~~~ v. 2021.1 ~~~~~
                 ****************************************************************


 ========================================================

 NAST &polynomial input group for Zhu-Nakamura
```

```
=======================================================

&polynomials
hs4 =  0.0914638
hs3 = -0.1206945
hs2 =  0.0930742
hs1 = -0.0040723
hs0 = -0.0000018
ls4 =  0.0000000
ls3 =  0.0000000
ls2 =  0.0000000
ls1 =  0.1269290
ls0 = -0.0487998
limitL =  0.00
limitR =  0.93
&end

==================

limitL & limitR

==================

limitR must be greater than limitL. limitL should be chosen at the reactant
minimum. Therefore, limitL is effectively zero: limitL = 0.0.

The choice of limitR depends on the intersection type.

For the sloped intersection, limitR should be chosen so that E1 = f(limitR) is well
above MECP to ensure convergence. For that, our default choice is limitR = 2.0 *
x_M, where x_M is the coordinate of MECP.

In this example, x_M was  0.47, E1(x_M) =  0.0104435 a.u. (  2292.08 cm-1).
Then, suggested limitR =  0.93, E1(limitR) =  0.0485754 a.u. (  10661.07 cm-1).

Fly with us again.
```

Plotted in the Figure 6.4 below are crossing potentials using polynomial coefficients calculated using the *ircfit* code.

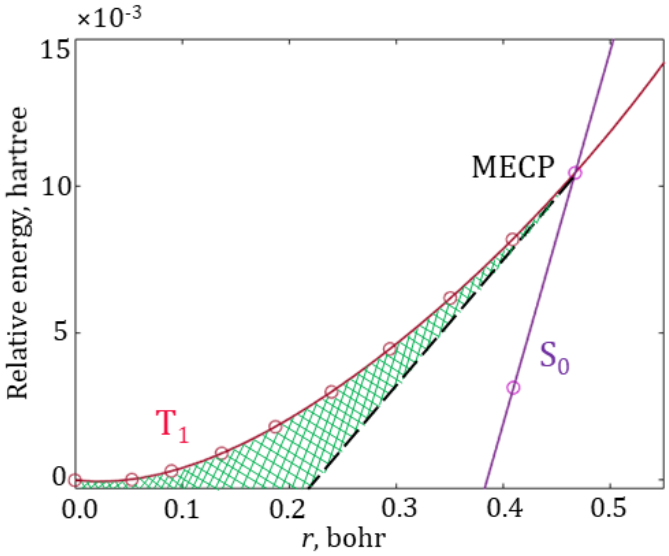

Figure 6.4. The fitted $T_1 \rightarrow MECP \rightarrow S_0$ reaction pathway. The circles mark the energies of the IRC geometries projected on the reaction coordinate *r*. Green area shows an increase in the tunneling barrier width compared to the linear model (dashed black line). The coefficients of the fitting polynomials ($f(x) = 0.092\,x^4 - 0.121\,x^3 + 0.093\,x^2 - 0.004\,x - 1.86 \times 10^{-6}$ and $g(x) = 0.127\,x - 0.048$) are included in the NAST input file.

The **&polynomials** group from the **.nast** file can be readily used as part of the input file for the NAST calculation. The parameters limitL and limitR set the left and right limits on the 1-D reaction coordinate. Effectively, they set the limits on the coordinate space where the potentials are scanned at each specific energy to calculate the ZN transition probability.

~~~~~~

Here ends the NAST package manual.

~~~~~~